Check for updates

N_2 binding to the E_0–E_4 states of nitrogenase†

Hao Jiang (ID) and Ulf Ryde (ID) *

Nitrogenase is the only enzyme that can convert N_2 into NH_3. The reaction requires the addition of eight electrons and protons to the enzyme and the mechanism is normally described by nine states, E_0–E_8, differing in the number of added electrons. Experimentally, it is known that three or four electrons need to be added before the enzyme can bind N_2. We have used combined quantum mechanical and molecular mechanics methods to study the binding of N_2 to the E_0–E_4 states of nitrogenase, using four different density functional theory (DFT) methods. We test many different structures for the E_2–E_4 states and study binding both to the Fe2 and Fe6 ions of the active-site FeMo cluster. Unfortunately, the results depend quite strongly on the DFT methods. The TPSS method gives the strongest bonding and prefers N_2 binding to Fe6. It is the only method that reproduces the experimental observation of unfavourable binding to the E_0–E_2 states and favourable binding to E_3 and E_4. The other three methods give weaker binding, preferably to Fe2. B3LYP strongly favours structures with the central carbide ion triply protonated. The other three methods suggest that states with the S2B ligand dissociated from either Fe2 or Fe6 are competitive for the E_2–E_4 states. Moreover, such structures with two hydride ions both bridging Fe2 and Fe6 are the best models for E_4 and also for the N_2-bound E_3 and E_4 states. However, for E_4, other structures are often close in energy, *e.g.* structures with one of the hydride ions bridging instead Fe3 and Fe7. Finally, we find no support for the suggestion that reductive elimination of H_2 from the two bridging hydride ions in the E_4 state would enhance the binding of N_2.

Introduction

Nitrogenase (EC 1.18/19.6.1) is the only enzyme that can cleave the triple bond in molecular N_2,[1–4] thereby making nitrogen available for biological lifeforms. X-ray crystallographic studies have shown that nitrogenase contains a complicated $MoFe_7S_9C$ (homocitrate) cluster in the active site, called the FeMo cluster (Fig. 1).[5–9] Alternative nitrogenases exist, in which the Mo ion is replaced by V or Fe, but they have lower activities.[10,11] The nitrogenase reaction is demanding, requiring eight electrons and 16 ATP molecules for each N_2 molecule processed:[3,4]

$$N_2 + 8e^- + 8H^+ + 16\ ATP \rightarrow 2\ NH_3 + H_2 + 16\ ADP + 16\ P_i \tag{1}$$
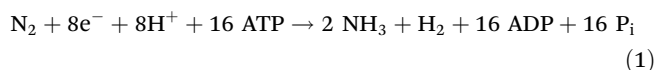
Nitrogenase has been extensively studied by spectroscopic, biochemical and kinetic methods.[1–9,12] The reaction is normally described by the Lowe–Thorneley cycle,[13] which involves nine intermediates, E_0–E_8, differing in the number of added electrons and protons. The E_0 resting state has been thoroughly characterised by crystallography, spectroscopic and compu-

tational studies.[4,7,14–16] The E_1 state has been studied by X-ray absorption and Mössbauer spectroscopy[17,18] and most likely contains a proton on the S2B μ_2 bridging sulfide ion (see Fig. 1b for atom names).[19] The E_2 state is known to involve two conformers, of which at least one contains an iron-bound hydride ion.[20–23] The E_4 state has been characterised by EPR and ENDOR spectroscopy, and has been shown to contain two hydride ions that bridge between two Fe ions of the FeMo cluster.[24–26] It has been shown that N_2 binds to the E_3 and E_4 states, but not the E_0–E_2 states.[1,25,27–30] In connection with the binding of N_2, H_2 is released by reductive elimination, *i.e.* by the formation of H_2 from two hydride ions.[25,26,31,32] Then, N_2 is successively reduced and protonated to two molecules of NH_3. Mutational studies have indicated that the Fe2–Fe3–Fe6–Fe7 face of the FeMo cluster is the primary site for N_2 reduction and that Fe2 or Fe6 are the most likely binding sites of N_2.[33,34]

Nitrogenase has also been extensively studied by computational methods, using density functional theory (DFT).[35] However, such studies are complicated by the fact that there are very many possibilities for the binding of up to four protons to the cluster, that different DFT method give widely different relative energies of the various protonation states and that the electronic structure is complicated (there are 35 possible broken-symmetry states).[35–38]

Several DFT studies have been devoted to the binding of N_2 to the FeMo cluster in different E_n states.[35] Early investigations

Department of Theoretical Chemistry, Lund University, Chemical Centre, P. O. Box 124, SE-221 00 Lund, Sweden. E-mail: Ulf.Ryde@teokem.lu.se; Fax: +46-46 2228648; Tel: +46-46 2224502

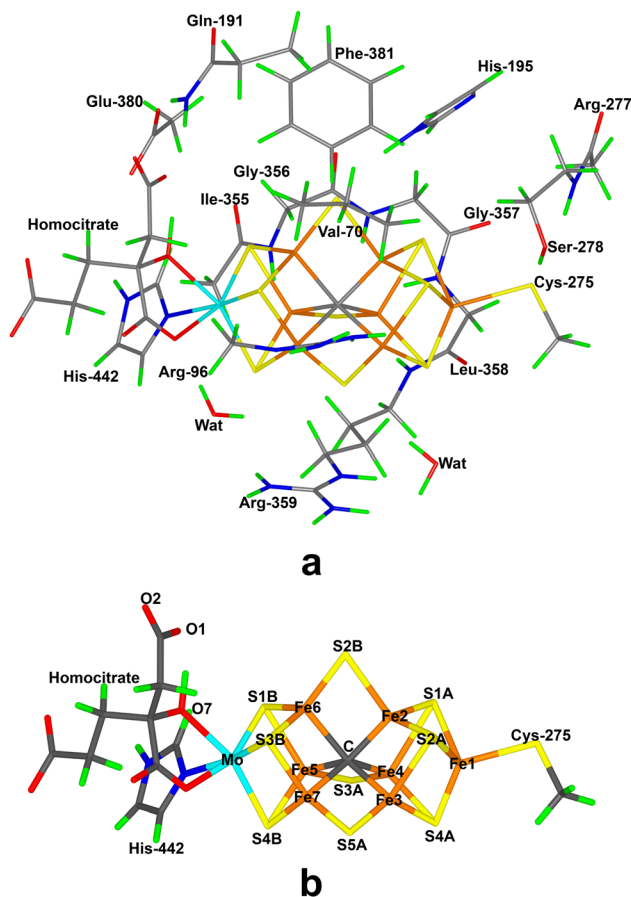†Electronic supplementary information (ESI) available. See DOI: https://doi.org/10.1039/d3dt00648d

Fig. 1 Structure of the FeMo cluster in the E_0 state. (a) Illustrates the QM system used in all calculations, as well as the names of the nearby residues; (b) shows the FeMo cluster with atom names indicated. H, C, N, O, S, Fe and Mo atoms are shown in green, grey, blue, red, yellow, orange and cyan, respectively. All figures show the same orientation and colouring scheme.

suffered from incomplete knowledge of the composition of the cluster, its net charge and the sequence of proton and N_2 binding.[39–42] However, also later studies have led to disparate suggestions. Blöchl, Kästner and coworkers suggested that N_2 binds to Fe7 after dissociation of S5A from this ion (atom names are shown in Fig. 1).[43,44]

Other groups have also suggested that such half-dissociation of the μ_2-bridging sulfide ions may enhance N_2 binding, but mainly for S2B and N_2 binding to Fe2 or Fe6,[45–47] and crystallographic studies have indicated that S2B may sometimes be replaced by other ligands,[8,48,49] indicating that sulfide lability may be mechanistically relevant.[50,51] In particular, Bjornsson and coworkers showed that N_2 may bind to Fe2 or Fe6 in E_4 with favourable binding energies of 56 or 43 kJ mol^{-1}, respectively.[52] They did not find any binding of N_2 to the E_0 and E_1 states, and a less favourable binding (29 kJ mol^{-1}) to the E_2 state. Recently, they have published a more thorough study, reporting unfavourable N_2-binding energies to E_0, E_1 and E_2 (by 69, 41 and 8 kJ mol^{-1}), but a slightly favour-

able binding energy to E_4, 17 kJ mol^{-1}.[53] They emphasize the importance of two doubly occupied 3d orbitals on the Fe ion binding N_2, which can donate electron density into the N_2 π^* orbitals.

Hoffman and coworkers have suggested that reductive elimination of H_2 from the E_4 state of nitrogenase is necessary for the binding of N_2.[54,55] Based on ENDOR experiments and DFT calculations, they suggested a structure of the E_4 state with two protons on S2B and S5A (both remaining bound to both Fe ions) and two hydride ions bridging Fe2/6 and Fe3/7, all located on the same face of the FeMo cluster. In such a structure, H_2 may form from the two hydride ions and N_2 can bind to this state with the concurrent release of H_2. DFT calculations suggested a favourable binding free energy of 13 kJ mol^{-1} and metadynamics simulations indicated that formation of H_2 is endergonic by 20 kJ mol^{-1}, with a barrier of 49 kJ mol^{-1} from the E_4 ground state.

Dance has presented several studies of N_2 binding to nitrogenase.[56–58] He showed that side-on binding of N_2 is less favourable than end-on binding and that N_2 bridging between two Fe ions is unfavourable. The early studies suggested preferable binding to Fe6. However, recently he suggested that first a promotional, but unreactive, N_2 binds to Fe2 in the exo-position and then a second reactive N_2 binds in the endo-position of Fe6.[59] He reported favourable binding energies of up to 38 kJ mol^{-1}. The binding is somewhat enhanced in structures with a bound H_2 molecule (up to 59 kJ mol^{-1}). In all structures, S2B remains bound to both Fe2 and Fe6.

On the other hand, Siegbahn argued that N_2 binding to the E_0–E_4 states is endergonic.[60,61] Therefore, he suggested that nitrogenase needs to be reduced by four additional electrons before it can bind N_2, i.e. that the E_0–E_3 states are outside the catalytic cycle and the E_4 state becomes the E_0 state in his catalytic cycle. Thereby, the cluster reaches a state with two Fe(I) ions and five Fe(II), which enhances binding of N_2. In his first study, N_2 was suggested to bind bridging between Fe4 and Fe6 in a reaction that is endergonic by 13 kJ mol^{-1}, but in a later study, he suggested that S2B dissociates from the cluster and N_2 binds to Fe4 with a slightly less endergonic free energy of 10 kJ mol^{-1}. The binding energy strongly depends on the amount of Hartree–Fock exchange in the functional.

Apparently, there is no consensus in how N_2 binds to the FeMo cluster and this is partly caused by the disagreement regarding the structure of the E_4 state and the large differences in the structures and energies obtained with different DFT functionals. Therefore, we here study the binding of N_2 to nitrogenase with four different DFT methods. We study the binding of N_2 to the five E_0–E_4 states and see how well different DFT functionals reproduce the experimental observation the N_2 binds only to the E_3 and E_4 states.[1,25,28–30] For the E_0–E_2 states, there is reasonable consensus regarding the preferred protonation states.[18,19,35,37,62,63] For the E_3 and E_4 states, we enhance previous studies of the preferred protonation state,[35,37,38,52,64–67] in particular with structures where S2B has dissociated from either Fe2 or Fe6.

Methods

The protein

The calculations are based on the 1.0 Å crystal structure of Mo nitrogenase from *Azotobacter vinelandii* (PDB code 3U7Q).[7] The setup of the protein is identical to that of our previous studies.[38,66,68,69] The entire heterotetramer was considered in the calculations and the quantum mechanical (QM) calculations were concentrated on the FeMo clusters in the C subunit because there is a buried imidazole molecule from the solvent rather close to the active site (~11 Å) in the A subunit. The two P clusters and the FeMo cluster in subunit A were modelled by MM in the fully reduced and resting states, respectively, using a QM charge model.[68] The protonation states of all residues were the same as before,[68] and the homocitrate ligand was modelled in the singly protonated state with a proton shared between the hydroxyl group (O7 that coordinates to Mo) and the O1 carboxylate atom.[16,68] The protein was solvated in a sphere with a radius of 65 Å around the geometrical centre of the protein. Cl^- and Na^+ ions were added to an ionic strength of 0.2 M.[70] The final system contained 133 915 atoms. For the protein, we used the Amber ff14SB force field[71] and water molecules were described by the TIP3P model.[72] The metal sites[68,73] were treated by a non-bonded model[74] and charges were obtained with the restrained electrostatic potential method.[75]

QM calculations

All QM calculations were performed with the Turbomole software (versions 7.5 and 7.6).[76] All structures were studied with the TPSS,[77] r^2SCAN,[78] TPSSh[79] and B3LYP[80–82] functionals. The former two are meta generalised gradient approximation (GGA) functionals, whereas the other two are hybrid functionals with 10 and 20% Hartree–Fock exchange, respectively. r^2SCAN and TPSSh have been shown to give very accurate structures of nitrogenase models.[83] We employed the def2-SV(P) basis set.[84] Previous studies have shown that increasing the basis set to def2-TZVPD changes the relative energies by up to 11–20 kJ mol^{-1}.[37,66,69,73] Test calculations for the best structures in this study, shown in Table S1 in the ESI,† confirm that this is also the case for the current structures (mean signed and unsigned changes of 2 and 6 kJ mol^{-1}), except in a few structures, in which the electronic structure changes extensively (Table S2†). However, for N_2-binding energies, the larger basis set gives more unfavourable binding energies by 9–21 kJ mol^{-1} (average 15 kJ mol^{-1}; *cf.* Table S3†), probably reflecting that the binding with the smaller basis set is enhanced by the basis-set superposition error. The calculations were sped up by expanding the Coulomb interactions in an auxiliary basis set, the resolution-of-identity (RI) approximation.[85,86] Empirical dispersion corrections were included with the DFT-D4 approach,[87] as implemented in Turbomole.

The FeMo cluster was modelled by MoFe$_7$S$_9$C(homocitrate) (CH$_3$S)(imidazole), where the two last groups are models of Cys-275 and His-442. In addition, all groups that form hydrogen bonds to the FeMo cluster were also included in the QM

model, *viz.* Arg-96, Gln-191 and His-195 (sidechains), Ser-278 (both sidechain and backbone, including some atoms from Arg-359), Gly-356, Gly-357 and Leu-358 (backbone), as well as two water molecules. Finally, the sidechain of Glu-380 was included because it forms hydrogen bonds to Gln191 and His-442, as well as the sidechains of Val-70 and Phe-381 because they are close to S2B, Fe2 and Fe6, *i.e.* the expected binding site of N_2. The QM system involved 189–195 atoms (depending on the E_n state and whether N_2 was included or not) and is shown in Fig. 1a. The net charge of QM region was always $-4e$. His-195 was always neutral and protonated on the NE2 atom, because this state has been found to be most stable in our previous studies.[37,68,88]

In this investigation we study the E_0–E_4 states of the FeMo cluster with or without N_2. The resting E_0 state has the formal $Mo^{III}Fe^{II}_3Fe^{III}_4$ oxidation state[14,16,89] and is a quartet state according to EPR experiments.[1–4] The other four states were obtained by successively adding one electron and one proton to the previous state. Several positions of the added protons were tested, based on previous investigations,[18,19,35,37,38,52,62–67] as will be discussed below. E_0 and E_2 were studied in the quartet spin state and E_4 in the doublet state, in agreement with experiments.[1–4,22,23,90] For E_1 and E_3, no experimental data are available and we assumed the quintet and triplet states (previous studies have shown that different spin states are close in energy).[37,63]

The electronic structure of all QM calculations was obtained with the broken-symmetry (BS) approach:[36] each of the seven Fe ions was modelled in the high-spin state, with either a surplus of α (four Fe ions) or β (three Fe ions) spin. Such a state can be selected in 35 different ways.[69] The various BS states were obtained either by swapping the coordinates of the Fe ions[91] or with the fragment approach by Szilagyi and Winslow.[92] The various BS states are named by listing the number in the Noodleman nomenclature (BS1–10),[36] followed by the numbers of the three Fe ions with minority spin. The selection of the BS states was based on our previous experience with the similar systems.[37,63,66] For E_0–E_2, we tested mainly the BS7-235 state. The E_3 structures were studied mainly in the BS10-147 state. For E_4, an initial investigation was performed in the BS10-147 and BS-14 states. For the best four (without N_2) or six (with N_2) structures, we tested eight additional BS states (BS7-235, BS7-247, BS7-346, BS2-234, BS6-157, BS8-347, BS10-127 and BS10-135) with all four functionals.

We study the binding of N_2 to nitrogenase. We will discuss three types of structures, *viz.* without any N_2 molecule (E_n), with N_2 bound directly to either Fe2 or Fe6 (denoted E_n–N_2), *i.e.* in the first coordination sphere with a Fe–N distance of typically 1.8–2.0 Å, but occasionally longer (especially with B3LYP), up to 2.5 Å (but with the N_2 molecule directed towards the Fe ion), or with N_2 unbound, but residing in the second coordination sphere of the Fe ion (denoted $E_n + N_2$). Naturally, the latter structures are less well defined, but stable structures were typically found with a Fe–N distance of ~3.7 Å from Fe6 and ~2.8 Å from Fe2. The N_2 molecule is no longer directed towards the Fe ion but forms weak dispersive interactions with

the surrounding residues. If no local minimum was found for either E_n–N_2 or E_n + N_2 (*i.e.* if the geometry optimisation converged to the other type), we obtained a structure with the Fe–N distance restrained to 1.9, 3.7 or 2.8 Å, for E_n–N, or second-sphere bonding to Fe6 and Fe2, respectively. Based on previous mutational and computational studies,[1–4,56–58] we study only binding to Fe2 or Fe6, and only end-on binding in the exo position (*i.e. trans* to the central carbide ion).

There are several ways to calculate N_2 binding energies. We use three different definitions in this article. First, we define the N_2 binding energy, ΔE_{N_2}, as the QM/MM energy difference between the N_2-bound structure and the best (*i.e.* the structure with the lowest QM/MM energy) optimised structure without N_2 at this E_n level (denoted $E_n(best)$), and a free N_2 molecule optimised in a conductor-like screening model (COSMO)[93,94] continuum solvent with a dielectric constant of 80, the default optimised COSMO atomic radius for N (1.83 Å) and a water solvent radius of 1.3 Å:[95]

$$\Delta E_{N_2} = E^{QM/MM}(E_n\text{–}N_2) - E^{QM/MM}(E_n(best)) - E^{COSMO}(N_2) \tag{2}$$

It should be noted that the COSMO solvation free energy of N_2 is only 2 kJ mol^{-1}, so it does not matter much whether it is calculated in vacuum or in the continuum solvent. This seems to be the definition used by Siegbahn[60,61] and by Bjornsson and coworkers in their latest study.[53]

Second, we define the direct N_2 binding energy (ΔE_{db}) as the difference in energy between the same type of structure (*i.e.* the same E_n and protonation state; denoted E_n + $N_2(same)$) with N_2 in the second or first coordination sphere:

$$\Delta E_{db} = E^{QM/MM}(E_n\text{–}N_2) - E^{QM/MM}(E_n + N_2(same)) \tag{3}$$

This is the definition used by Dance.[59] We have also followed such binding reactions by starting from the second-sphere structure and adding a restraint on the Fe–N distance, which is successively decreased to a typical bonding distance (~1.9 Å) and finally removing the restraints. The resulting potential-energy surfaces also give approximate activation energies for the binding, which are reported.

A third way to define binding energies, intermediate between the other two, is to use the same type of complex without N_2 bound (*i.e.* the same E_n and protonation state; denoted $E_n(same)$) and free N_2 as the reference:

$$\Delta E_{bn} = E^{QM/MM}(E_n\text{–}N_2) - E^{QM/MM}(E_n(same)) - E^{COSMO}(N_2) \tag{4}$$

This seems to be the definition used by Bjornsson and co-workers in their first study[52] and called single-step N_2 binding energy in their second study.[53] In all three cases, a negative binding energy indicates a favourable binding.

QM/MM calculations

QM/MM calculations were performed with the ComQum software.[96,97] In this approach, the protein and solvent are split into two subsystems: system 1 (the QM region) was relaxed by QM methods, whereas system 2 contained the remaining part of the protein and the solvent, and it was kept fixed at the original coordinates (equilibrated crystal structure, to avoid the risk that different calculations end up in different local minima).

In the QM calculations, system 1 was represented by a wavefunction, whereas all the other atoms were represented by an array of partial point charges, one for each atom, taken from the MM setup. Thereby, the polarisation of the QM system by the surroundings is included in a self-consistent manner (electrostatic embedding). When there is a bond between systems 1 and 2 (a junction), the hydrogen link-atom approach was employed: the QM system was capped with hydrogen atoms, the positions of which are linearly related to the corresponding carbon atoms (carbon link atoms, CL) in the full system.[96,98] All atoms were included in the point-charge model, except the CL atoms.[99] ComQum employs a subtractive scheme with van der Waals link-atom corrections.[100] No cut-off is used for any of the QM or MM interactions. The geometry optimisations were continued until the energy change between two iterations was less than 2.6 J mol^{-1} (10^{-6} a.u.) and the maximum norm of the Cartesian gradients was below 10^{-3} a.u. Approximate transition states for the binding N_2 were obtained by first optimising free N_2 at a distance of 2.5–4 Å from Fe2 or Fe6 and then performing a relaxed scan of Fe–N distances until a bound state was found.

Results and discussion

We have studied the binding of N_2 to the FeMo cluster in nitrogenase. We will discuss the results for different E_n states in separate sections.

N_2 binding to the E_0 and E_1 states

We first studied the binding of N_2 to the resting E_0 state of nitrogenase (using BS7-235;[69] shown in Fig. 1b). As expected, no N_2-bound state was found with any of the four DFT methods. Bonded structures could be obtained by restraining the Fe–N distance of 1.90 Å. However, the binding energy for such restrained structures is unfavourable, more for the binding to Fe2 than to Fe6, *e.g.* ΔE_{N_2} = 44 and 34 kJ mol^{-1} for TPSS (*cf.* Table 1). With the other three functionals, the energies are slightly more unfavourable, 44–61 kJ mol^{-1} for Fe6 and 49–69 kJ mol^{-1} for Fe2, with the trend B3LYP < TPSSh < r²SCAN.

For the E_1 state, we added the proton to S2B in agreement with previous QM/MM[35,37] and experimental studies.[18,19] We assumed that the proton points towards S3A and that the FeMo cluster remains in the BS7-235 state.[35,37,69]

In this case, a state with N_2 bound end-on to both Fe2 and Fe6 could be found with TPSS (Fig. 2). They have both a Fe–N distance of 1.92 Å (*cf.* Table 1). However, the ΔE_{N_2} binding energies are still unfavourable, by 26 and 33 kJ mol^{-1} for Fe6 and Fe2, respectively. A state with N_2 in the second coordination sphere of Fe6 (with a Fe6–N distance of 3.68 Å, Fig. 2)

Table 1 Structures of the E_0 and E_1 states with N_2 in the second coordination sphere ($+N_2$) or bound ($-N_2$) to either Fe2 or Fe6. For each structure and each of the four DFT methods, the Fe–N bond length (in Å; bold face indicates a restrained distance), the relative energy (ΔE in kJ mol^{-1}, within the same column and section) and the ΔE_{N_2} binding energy (eqn (2) in kJ mol^{-1}). Fe–N$_{TS}$ and ΔE_{TS} are the bond length and activation energy for the transition state for the binding of N_2. All structures were studied in the BS7-235 state. All E_1 structures were protonated on S2B, with the proton directed towards S3A

|		TPSS					r^{2}SCAN			TPSSh			B3LYP		
E_n	Struct.	Fe–N	ΔE	ΔE_{N_2}	Fe–N$_{TS}$	ΔE_{TS}	Fe–N	ΔE	ΔE_{N_2}	Fe–N	ΔE	ΔE_{N_2}	Fe–N	ΔE	ΔE_{N_2}
E_0	Fe2 + N$_2$	2.79	27.6	28.6				39.4	35.8		31.6	33.3		37.7	35.1
	Fe6 + N$_2$	3.31	0.0	1.0				0.0	−3.6		0.0	1.6		0.0	−2.5
	Fe2–N$_2$	**1.90**	42.6	43.5			**1.90**	69.0	65.4	**1.90**	60.0	61.6	**1.90**	49.5	46.9
	Fe6–N$_2$	**1.90**	33.4	34.3			**1.90**	60.9	57.3	**1.90**	56.0	57.7	**1.90**	44.0	41.5
E_1	Fe2 + N$_2$	2.84	31.0	32.8	2.4	39.7	2.86	39.1	37.4	2.81	32.0	35.4	2.83	39.0	39.1
	Fe6 + N$_2$	3.68	0.0	1.9	2.0	32.4	3.63	0.0	−1.7	3.64	0.0	3.4	3.63	0.0	0.1
	Fe2–N$_2$	1.92	31.1	32.9			1.97	42.9	41.2	2.01	46.4	49.9	**1.90**	80.8	80.9
	Fe6–N$_2$	1.92	24.1	26.0			**1.90**	60.3	58.6	**1.90**	58.6	62.1	**1.90**	73.7	73.9
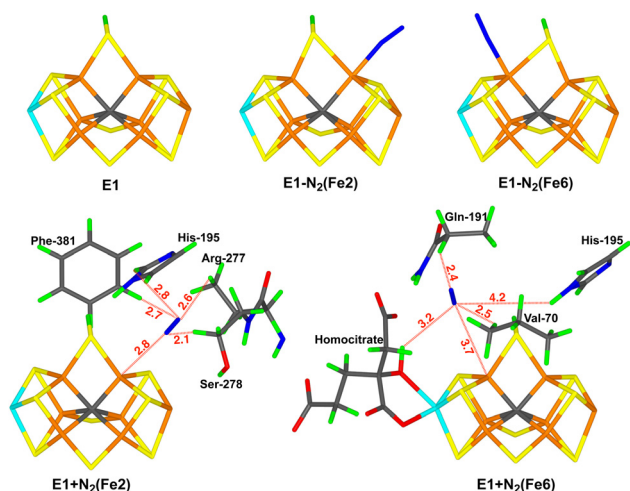
Fig. 2 The best E_1 structures, obtained with TPSS: E_1 without N_2, Fe2–N_2 and Fe6–N_2 with N_2 coordinating to Fe, as well as Fe2 + N_2 and Fe6 + N_2 with N_2 in the second coordination sphere, showing also nearby residues.

has $\Delta E_{N_2} = 2$ kJ mol^{-1}, showing that we could also have used such a structure as the reference state. In this structure N_2 resides in a cavity between homocitrate, His-195, Gln-191 and Val-70, forming weak interactions with in particular the latter two residues (N···H distances of 2.4–4.2 Å). The activation energy for the binding of N_2 to Fe6 from this second-sphere structure is only 32 kJ mol^{-1}.

Around Fe2, a second-sphere structure with a Fe2–N distance of 2.84 Å can be found, but it is 31 kJ mol^{-1} less favourable ($\Delta E_{N_2} = 33$ kJ mol^{-1}; Fig. 2). On the other hand, binding from this structure to Fe2 has an activation energy of only 9 kJ mol^{-1}. In this structure, N_2 interacts weakly with Ser-278 (2.1 Å), Arg-277 (2.6 Å), Phe-381 (2.7 Å) and His-195 (2.8 Å).

With the other three functionals, no structure with N_2 bound to Fe6 was found. However, structures with N_2 bound to Fe2 were found for TPSSh and r^{2}SCAN, but not with B3LYP. They have Fe2–N distances of 1.97 and 2.01 Å, and ΔE_{N_2}

unfavourable binding energies of 41 and 50 kJ mol^{-1} for r^{2}SCAN and TPSSh, respectively. Restraining the Fe–N distance to 1.90 Å, we obtain a ΔE_{N_2} binding energy for B3LYP of 81 kJ mol^{-1}. For Fe6, such restrained structures give $\Delta E_{N_2} = 59$–74 kJ mol^{-1}. For B3LYP, binding to Fe6 is stronger, whereas for the other two functionals binding to Fe2 is stronger. Thus, we can conclude that all four functionals suggest that N_2 binding to the E_0 and E_1 states is unfavourable, in agreement with experiments.[1,25,28–30] For E_1, the bond strengths are in the order TPSS > r^{2}SCAN > TPSSh > B3LYP, showing a decreasing trend with respect to the amount of HF exchange in the functional (10% for TPSSh and 20% with B3LYP).

N_2 binding to the E_2 state

Next, we considered the binding of N_2 to the E_2 state. We first studied ten structures for the unligated E_2 state with the H atoms on S2B, S5A, Fe5, the central carbide or bridging Fe2 and Fe6 (denoted Fe2/6). In some structures, the protonated S2B group had dissociated from either Fe2 or Fe6. The structures are described in Table 2 and are shown in Fig. 3. Most of them were included also in our previous study[63] and we use the naming convention from that study (explained in detail in Table 2): Structures starting with a "B" have a hydride ion _bridging_ Fe2 and Fe6, and S2B is protonated and also _bridging_ Fe2 and Fe6. The two numbers indicate the direction of the proton on S2B and the hydride ion (in this order), _viz._ pointing towards S3A(3) or towards S5A(5). Structures starting with "H" has the proton and the hydride in the same positions, but S2B has dissociated from either Fe2 or Fe6, but not the other Fe ion (it is _half-dissociated_). The number indicates which Fe ion it still binds to, and the final letter indicates whether the proton on S2B points towards Fe, S or Mo. Structures starting with "N" have _no_ bridging hydride ion, but instead protons on S2B and S5A. The numbers indicate the direction of the two protons in this order (for that on S5A, either towards S2B or S5A). The T53 structure has a _terminal_ hydride ion on Fe5 and a proton on S2B, directed towards S3A. The C2 structure had a doubly protonated central _carbide_ ion.

Dalton Transactions

Paper

Table 2 The ten structures studied for the E_2 state without N_2. The names are the same as in our previous study of this state.[63] ΔE is the relative energy for each DFT method (kJ mol^{-1}). The H1 and H2 columns describe which atom is protonated and the direction of the proton. S2B (3) or S2B(5) means that S2B is protonated with the proton directed towards the S3A or S5A atoms. Fe2/6(5) means that the H atom bridges Fe2 and Fe6 on the same side of S2B as S5A. C2367 and C3457 means that the central carbide is protonated with the proton pointing to the Fe2–Fe3–Fe6–Fe7 or Fe3–Fe4–Fe5–Fe7 face. S2B(H6S) means that S2B is protonated and is dissociated from Fe2, but remains bound to Fe6, with the proton directed towards S1B. Likewise, S2B(H2F) means that S2B is protonated and is dissociated from Fe6, but remains bound to Fe2, with the proton directed towards Fe1. The structures were studied in the BS7-235 state, unless otherwise stated

Structure	H1	H2	ΔE (kJ mol^{-1})			
			TPSS	r^{2}SCAN	TPSSh	B3LYP
B33	S2B(3)	Fe2/6(3)	0.0	41.0	14.5	55.0
B35	S2B(3)	Fe2/6(5)	17.0	16.7	9.5	44.5
B53	S2B(5)	Fe2/6(3)	4.4	46.0	20.6	63.9
B55	S2B(5)	Fe2/6(5)	32.7	62.6	42.3	82.8
H6S	S2B(H6S)	Fe2/6	13.3	0.0	0.0	0.0[a]
H2F	S2B(H2F)	Fe2/6	75.3	79.6	70.8	97.4
N33	S2B(3)	S5A(3)	26.4	54.6	24.5	27.0
N52	S2B(5)	S5A(2)	45.7	77.1	45.8	44.5
T53	S2B(3)	Fe5	19.0	24.9	16.0	26.8
C2[b]	C2367	C3457	157.7	113.1	35.1	−88.5

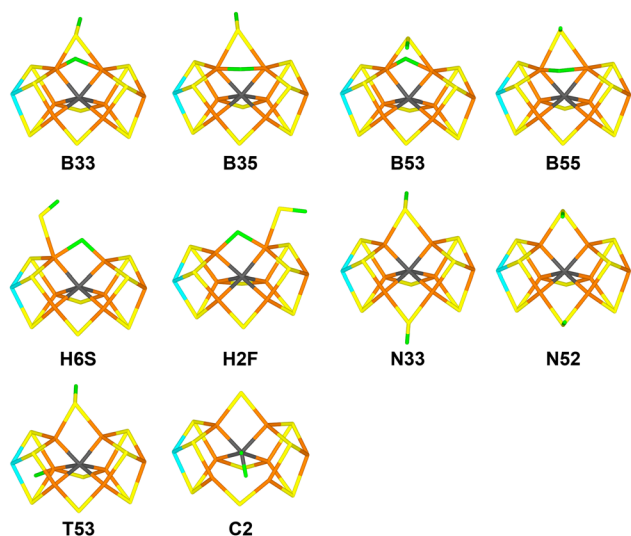[a] Studied in the BS7-346 state. [b] Studied in the BS8-345 state.

Fig. 3 The ten E_2 structures without N_2 bound. The positions of the added H atoms are described in Table 2 and the labels are explained in the text.

The relative stabilities of these structures are also shown in Table 2. It can be seen that with the TPSS functional, the B33 structure (with H atoms on S2B and bridging Fe2/6; Fig. 3) is most stable, 13 kJ mol^{-1} better than the half-dissociated H6S structure (with H atoms in the same positions, but with S2B dissociated from Fe2; Fig. 3). With the other three functionals,

the situation is opposite by 14–55 kJ mol^{-1} (in both cases, some other structures are intermediate in energy). However, with B3LYP, the structure with the central carbide ion doubly protonated (C2; Fig. 3) is 88 kJ mol^{-1} more stable, whereas this structure is disfavoured by 35–158 kJ mol^{-1} with the other functionals. Such structures are strongly distorted.

Next, we studied the binding of N_2 to the best of these structures. The results are collected in Table 3. With the TPSS functional, N_2 was found to bind to both Fe2 and Fe6 for all types of structures. The most favourable structure has N_2 bound to Fe6 and S2B bound to Fe2 but dissociated from Fe6 (Fig. 4). Such a structure naturally forms from the H2F structure, but it arose also from the B33 and B35 structures, because S2B automatically dissociated from Fe6 during the binding of N_2 (the three structures are isoenergetic within 0.5 kJ mol^{-1} and we describe the best, Fe6–B35, in the following). It has a Fe6–N bond length of 1.81 Å and a favourable ΔE_{N_2} of −11 kJ mol^{-1}. The corresponding structure with N_2 bound to Fe2 and S2B bound only to Fe6 is 7 kJ mol^{-1} less stable (H6S; again it arose also from B33 or B35 by spontaneous S2B dissociation from Fe2; Fig. 4). The Fe2–N bond length is 1.85 Å and ΔE_{N_2} is −5 kJ mol^{-1}. Structures with S2B still bridging both Fe2 and Fe6 are 52–67 kJ mol^{-1} less stable when N_2 binds to Fe6 and 64–78 kJ mol^{-1} less stable when N_2 binds to Fe2, in both cases following the order N33 < T53 < N52. Structures with N_2 binding in the second sphere can be found for all structures, except H6S and H2F, but they are 30–78 kJ mol^{-1} less stable than the best bound N_2-bound structure. The activation energy for N_2 binding is rather small for all structures, 5–46 kJ mol^{-1}, and barrierless in three cases.

With the other three DFT functionals, N_2 does not bind to Fe6 for the N33 and N52 structures, and it does not bind to Fe2 for the T53 structure (very weakly for B3LYP with a Fe2–N distance of 2.42 Å). In fact, most B3LYP structures with N_2 binding to Fe2 have very long Fe2–N distances, 2.28–2.53 Å (1.98–2.15 Å, 2.01–2.02 Å and 1.85–1.95 Å for the corresponding structures with TPSSh, r^{2}SCAN and TPSS, respectively). As with TPSS, S2B dissociates from the Fe ion binding N_2 for the B33 and B35 structures, giving structures virtually identical to those started from the half-dissociated H6S or H2F structures. The same happens for N_2 binding to Fe6 in the T53 structure with all three functionals and for N_2 binding to Fe2 in the N33 and N52 structures with r^{2}SCAN and TPSSh. With
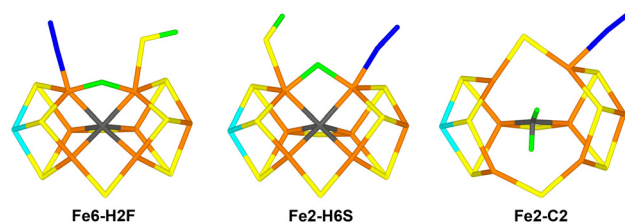

Fig. 4 The best E_2 structures with N_2 bound, Fe6–H2F, Fe2-H6S and Fe2–C2. The first two were optimised with TPSS, whereas Fe2–C2 was optimised with B3LYP.

Table 3 Structures studied for the E_2 state with N_2. The structures are the same as in Table 2 and the entries are the same as in Table 1. ΔE_{db} is the direct binding energy relative to the same type of structure with N_2 in the second sphere (upper part of the table; eqn (3)). All Fe–N bond lengths are in Å (a distance in bold face indicates a restrained bond) and all energies in kJ mol^{-1}. All structures were studied in the BS7-235 state, if not otherwise stated

Structure		TPSS Fe–N	TPSS ΔE	TPSS ΔE_{N_2}	TPSS ΔE_{db}	FeN$_{TS}$	ΔE_{TS}	r2SCAN Fe–N	r2SCAN ΔE	r2SCAN ΔE_{N_2}	r2SCAN ΔE_{db}	TPSSh Fe–N	TPSSh ΔE	TPSSh ΔE_{N_2}	TPSSh ΔE_{db}	B3LYP Fe–N	B3LYP ΔE	B3LYP ΔE_{N_2}	B3LYP ΔE_{db}
Fe2 + N2	B33	2.86	55.0	43.6				2.85	55.6	70.1		2.88	58.0	66.7		2.87	66.1	193.5	
	B35	2.80	63.8	52.4				2.04	6.9	21.5		2.08	12.6	21.4		2.46	9.7	137.0	
	T53	2.89	62.7	51.3				2.91	53.7	68.3		2.87	48.8	57.6		2.81	65.7	193.0	
	N33	2.81	69.5	58.1				2.79	77.6	92.2		2.70	50.1	58.9		2.64	18.6	145.9	
	N52	2.89	78.2	66.7				2.86	89.5	104.0		2.80	62.7	71.5		2.80	31.1	158.4	
	H6S	**2.80**	48.3	36.9				**2.80**	13.5	28.1		**2.80**	19.3	28.1		**2.80**	4.5	131.8	
	C2	2.75^a	192.1	180.7				2.70^a	128.1	142.7		2.70^a	55.1	63.9		2.86	−95.7	31.7	
Fe6 + N2	B33	3.40	29.8	18.4				3.54	25.7	40.3		3.42	31.7	40.5		3.50	33.5	160.8	
	B35	3.56	34.1	22.7				3.52	4.9	19.5		3.52	8.7	17.5		3.51	12.6	139.9	
	T53	3.66	34.0	22.6				3.61	8.9	23.4		3.66	11.9	20.6		3.60	−10.4	116.9	
	N33	3.60	42.2	30.8				3.58	40.7	55.2		3.56	21.8	30.5		3.50	−16.9	110.4	
	N52	3.24	56.1	44.7				3.35	60.0	74.6		3.25	40.9	49.6		3.36	5.2	132.5	
	H2F	**3.70**	76.7	65.3				**3.70**	46.8	61.4		**3.70**	49.6	58.4		**3.70**	44.2	171.5	
	C2	3.20^a	169.9	158.4				3.32^a	93.2	107.7		3.27^a	26.7	35.5		3.22	−135.8	−8.5	
Fe2–N2	B33^b	1.85	7.0	−4.4	−48.0	2.40	4.9	2.01	2.1	16.7	−53.5	2.00	2.1	10.9	−55.9	2.52	1.6	128.9	−8.1
	B35^b	1.85	6.9	−4.5	−56.9	No barrier		2.01	0.0	14.6	−6.9	1.98	0.0	8.8	−12.6	2.53	0.0	127.3	−9.7
	T53^c	1.91	66.6	55.1	3.9	2.30	12.2	**1.90**	75.4	90.0	21.7	**1.90**	86.3	95.1	37.5	2.42	67.7	195.0	2.0
	N33	1.93	63.9	52.5	−5.6	2.40	4.6	2.01^b	77.9	92.5	0.3	2.15^b	47.6	56.4	−2.5	2.28	16.1	143.4	−2.6
	N52	1.95	78.5	67.1	0.3	2.30	7.3	2.02^b	89.6	104.1	0.1	2.14^b	64.2	73.0	1.5	2.30	31.3	158.6	0.2
	H6S	1.85	6.7	−4.7	−41.6	No barrier		2.01	2.1	16.6	−11.5	2.00	1.2	10.0	−18.1	2.01	1.8	129.1	−2.7
	C2	2.29^a	184.8	173.4	−7.3	2.30	11.0	2.54^a	126.2	140.8	−1.9	2.35^a	56.5	65.3	1.4	2.11	−105.3	22.0	9.6
Fe6–N2	B33^b	1.80	0.4	−11.0	−29.4	2.30	46.4	1.83	32.6	47.2	6.9	1.83	34.0	42.8	2.4	1.93	74.3	201.6	40.8
	B35^b	1.81	0.0	−11.4	−34.1	2.30		1.87	20.6	35.2	15.7	1.86	21.9	30.7	13.2	1.98	51.2	178.5	38.6
	T53	1.83	56.9	45.5	22.9	2.20	16.4	1.86^b	121.3	135.9	112.5	1.86^b	102.2	111.0	90.4	1.89^b	151.3	278.7	161.8
	N33	1.88	51.6	40.2	9.4	2.30	14.0	**1.90**	75.1	89.7	34.4	**1.90**	57.1	65.9	38.3	**1.90**	46.8	174.2	61.2
	N52	1.95	66.9	55.5	10.8			**1.90**	92.8	107.4	32.8	**1.90**	72.9	81.7	32.1	**1.90**	59.2	186.5	53.9
	H2F	1.81	0.5	−10.9	−76.2	No barrier		1.87	19.9	34.5	−26.9	1.85	19.3	28.1	−30.4	1.96	51.0	178.3	6.8
	C2	1.81	175.5	164.1	37.3			2.08^a	97.5	112.1	4.4	2.13	46.2	55.0	−0.6	1.81^a	6.2	133.5	136.4

^{a} Studied in the BS8-345 state. ^{b} S2B dissociates spontaneously from the Fe ion not binding N_2. ^{c} Studied in the BS10-147 state.

the latter two functionals, the most favourable structure is Fe2-H6S (which arises also from B33 and N35). This structure is 20 and 19 kJ mol^{-1} more stable than the corresponding structure with N_2 bound to Fe6 (Fe6-H2F/B33/B35; which was most stable with TPSS), respectively. ΔE_{N_2} of the best structure is unfavourable by 9–15 kJ mol^{-1}. Second-sphere N_2 binding is found to both Fe2 and Fe6 for all structures except H6S and H2F. The best is Fe6 + B35, but the corresponding Fe2 structure is only 2–4 kJ mol^{-1} less stable. They are 5–9 kJ mol^{-1} less stable the best first-sphere N_2-bound structure.

With B3LYP, the structure with N_2 binding to Fe2 in the C2 structure is by far most stable, 105 kJ mol^{-1} more stable than the Fe2-H6S (or B33 or B35) structure (Fig. 4). However, the ΔE_{N_2} binding energy is unfavourable by 22 kJ mol^{-1}.

It is notable that for several structures, the direct N_2 binding energy ΔE_{db} is favourable for all four methods, by up to 76, 53, 56 and 10 kJ mol^{-1} for TPSS, r^{2}SCAN, TPSSh and B3LYP, respectively. However, this mainly reflects problems with the definition of ΔE_{db}. For r^{2}SCAN and TPSSh, the strongly favourable ΔE_{db} energies comes from the B33 structure, which reorganises to a H6S structure when N_2 binds (by dissociation of S2B from one of the Fe ions). If we instead use the (restrained) H6S structure as the reference, ΔE_{db} becomes much less favourable, −11 and −18 kJ mol^{-1}. For TPSS, favourable ΔE_{db} are also obtained for structures in which S2B is already half-dissociated, for which no minimum with N_2 in the second coordination sphere is found. The large difference between ΔE_{db} and ΔE_{N_2} is caused by the unfavourable energies of all structures with N_2 in the second coordination sphere. In reality, the binding takes place to the most stable E_2 structure without N_2 and forms the most stable E_2–N_2 structure (unless kinetic barriers are large). Therefore, ΔE_{N_2} of the best E_2–N_2 structure should be the most relevant binding energy and we will not discuss ΔE_{db} for the other E_n states (it is still included in the tables).

N_2 binding to the E_3 state

Next, we turn to the E_3 state. This state is less thoroughly studied than the other states.[37] However, the results from the E_2 and E_4 states give some clues of possible protonation states also for E_3.[18,19,35,37,38,52,54,62–67] We have optimised 16 different structures without N_2. The protonation states and the nomenclature are described in Table 4 and the structures are shown in Fig. 5. Two types of structures were studied. One is based on the suggestions by Hoffman and coworkers[54] that E_4 has protons on S2B and S5A, as well as two hydride ions bridging Fe2/6 and Fe3/7. Each H atom can attain two conformations, *e.g.* directed towards S3A or S5A for the one on S2B (but the hydride ion on Fe3/7 was always on the S2B side of S5A). This gives eight possibilities for E_4 and we studied six variants of these with either the H atom on Fe3/7 or S5A is deleted for E_3. They are denoted in the same way as for E_4 below, *i.e.* with four numbers showing the conformation of the H atoms on S2B, Fe2/6, Fe3/7 and S5A in this order, using underscore to indicate a vacancy, *e.g.* 332_. Two variants of the 35_3 structure were also studied with S2B dissociated from either Fe2 or Fe6, but still binding to Fe6 (H6S) or to Fe2 (H2F; the final letter reflect the direction of the proton on S2B, towards S or Fe). The second type of structures is based on the suggestion by Bjornsson and coworkers that two hydride ions may both bridge Fe2/6, especially if S2B is protonated and has dissociated from either Fe2 or Fe6.[62] The names of these structures start with a "S" (the hydride ions bind the *same* pair of Fe ions). Four such structures were studied, depending on the direction of the proton on S2B (S2F, S2S, S6M and S6S, indicating that the proton points towards Fe, S or Mo). In addition, a structure with the central carbide ion triply protonated (C3) and three structures with hydride ions terminally bound on one or two Fe ions were studied (345, 335 and 355; explained in Table 4).[37]

Table 4 The 16 structures studied for the E_3 state without N_2. ΔE is the relative energy for each DFT method (kJ mol^{-1}). The H1, H2 and H3 columns describe which atom is protonated and the direction of the proton in the same way as was described in the legend of Table 2. The structures were studied in the BS10-147 state, unless otherwise stated

Structure	H1	H2	H3	ΔE (kJ mol^{-1})			
				TPSS	r^{2}SCAN	TPSSh	B3LYP
352_	S2B(3)	Fe2/6(5)	Fe3/7(2)	43.5	77.5	62.4	86.7
35_2	S2B(3)	Fe2/6(5)	S5A(2)	42.1	56.1	31.7	0.0
35_3	S2B(3)	Fe2/6(5)	S5A(3)	32.2	45.1	20.9	9.3
H2F	S2B(H2F)	Fe2/6	S5A(3)	101.1	109.3	81.8	70.4
H6S	S2B(H6S)	Fe2/6	S5A(3)	57.0	64.8	50.8	31.0
552_	S2B(5)	Fe2/6(5)	Fe3/7(2)	58.8	94.3	79.4	104.0
55_2	S2B(5)	Fe2/6(5)	S5A(2)	60.5	76.5	51.1	34.2
55_3	S2B(5)	Fe2/6(5)	S5A(3)	49.9	64.7	39.9	28.0
345	S2B(3)	Fe4	Fe5	54.1	58.1	58.0	70.1
335	S2B(3)	Fe2/6(3)	Fe5	47.7	69.3	55.6	80.2
355	S2B(3)	Fe2/6(5)	Fe5	42.1	58.4	44.3	64.1
S2F	S2B(H2F)	Fe2/6	Fe2/6	45.3	66.9	51.8	84.7
S2S	S2B(H$_2$S)	Fe2/6	Fe2/6	49.7	69.6	56.7	88.9
S6M	S2B(H6M)	Fe2/6	Fe2/6	1.3^a	1.8	9.1	28.1
S6S	S2B(H6S)	Fe2/6	Fe2/6	0.0	0.0	0.0	16.7
C3	C2367	C2456	C3457	175.8	141.1	3.6^b	−177.9

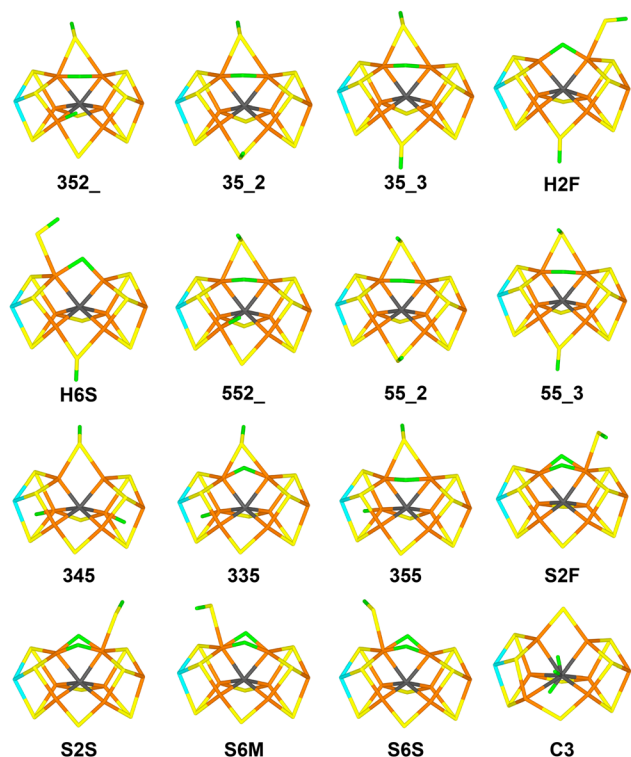^{a} Studied in the BS-14 state. ^{b} Studied in the BS10-136 state.

Fig. 5 The 16 E_3 structures without N_2 bound. The positions of the added H atoms are described in Table 4 and the nomenclature is explained in the text.

The relative stabilities of these structures are shown in Table 4. It can be seen that with TPSS, r^2SCAN and TPSSh, the S6S structure is most stable, *i.e.* with two Fe2/6 hydride ions and S2B protonated and binding only to Fe6 (Fig. 5). The S6M structure with the proton on S2B pointing in a different direction is close in energy (1–9 kJ mol^{-1}). The third-best state is 35_3 (H atoms on S2B(3), Fe2/6(5) and S5A(3); Fig. 5), which is 32, 45 and 21 kJ mol^{-1} less stable with the three functionals, respectively. With B3LYP, instead the C3 structure is best (with a triply protonated carbide ion; Fig. 5), 178 and 195 kJ mol^{-1} more stable than the 35_2 and S6S structures. The C3 structure is only 4 kJ mol^{-1} less stable than S6S with TPSSh, whereas it is 176 and 141 kJ mol^{-1} less stable with TPSS and r^2SCAN, confirming the previous observation[38] that the stability of structures with the central carbide protonated depends strongly on the amount of HF exchange in the functional. Interestingly, no functional indicates that the half-dissociated variants of 35_3 (H2F and H6M) are more stable than non-dissociated variant.

For the most stable and interesting structures, we then studied binding of N_2 (results in Table 5). All tested structures gave stable N_2-bound states at both Fe ions, except Fe6-35_2. With r^2SCAN, no 345 structure with N_2 bound to Fe2 or Fe6 was found. For the 355, 35_2, 35_3 and 352_ structures with N_2 binding to Fe2, S2B dissociated from Fe2. With TPSS, the most stable structure was S2S with N_2 bound to Fe6 (Fig. 6). It gave a Fe–N bond length of 1.80 Å. ΔE_{N_2} is favourable by 46 kJ mol^{-1}. The other three structures with two hydrides bridging Fe2/6 (S2F, S6M and S6S) are rather close in energy (14–23 kJ mol^{-1} less stable), whereas the other structures are appreciably worse (at least 66 kJ mol^{-1} less stable than Fe6-S2S).

With r^2SCAN and TPSSh, instead the two S6M and S6S structures with N_2 bound to Fe2 (Fig. 6) are most stable and degenerate within 1 kJ mol^{-1}. They have Fe–N bond lengths of 1.84 Å, but unfavourable ΔE_{N_2} = 9 or 3 kJ mol^{-1}, respectively. The Fe6-S2S structure is 21–30 kJ mol^{-1} less stable and the Fe2-35_3 structure (with S2B dissociated from Fe2; Fig. 6) is 28 (TPSSh) or 48 (r^2SCAN) kJ mol^{-1} worse.

With B3LYP, the situation is similar: Fe2-35_3 and Fe6-S2S are 9 and 27 kJ mol^{-1} less stable than Fe2-S6S, the latter with a Fe–N bond length of 1.88 Å. However, the C3 structures are by far the most stable, by 180 and 164 kJ mol^{-1} for N_2 bound to Fe2 and Fe6, respectively (Fig. 6). For the latter two, ΔE_{N_2} is unfavourable by 28–44 kJ mol^{-1}.

Structures with N_2 in the second coordination sphere of the Fe6 ion were found for most structures, but not for the C3 structure or for any of the structures with two Fe2/6 hydride ions. With N_2 in the second coordination sphere of Fe2, only three structures were found, 345, 355 and 35_2. These structures are much less stable than the N_2-bound structures with TPSS, r^2SCAN and TPSSh (by at least 76, 39 and 26 kJ mol^{-1}). However, with B3LYP, they are slightly more stable than the corresponding N_2 bound structures (by up to 15 kJ mol^{-1}), but they are still much less stable than the N_2-bound C3 structures (for which no second-sphere structures are found; by 165 kJ mol^{-1}). Activation barriers for the binding of N_2 from the second coordination sphere are low, 4–35 kJ mol^{-1}, and many of the reactions are barrierless (*cf.* Table 5).

N_2 binding to the E_4 state

Finally, we studied also the E_4 state using 20 different structures, described in Table 6 and shown in Fig. 7. The naming of the structures follows the same philosophy as for the E_3 structures and in analogy with these, we investigated mainly two types of structures. The first is structures with protons on S2B and S5A and two hydride ions bridging Fe2/6 and Fe3/7, as suggested by Hoffman and coworkers.[54] We studied eight such structures with the H atoms pointing in different directions,[66] as is described in Table 6 and Fig. 7. The 5522 structure is the one advocated by Hoffman and coworkers,[54] whereas the 3323 structure was lowest in energy in our previous study.[66] We also studied four variants of these with the protonated S2B group dissociated from either Fe2 or Fe6 (H6 or H2). Second, we studied six structures with two protons still on S2B and S5A, but both hydride ions bridging Fe2/6 and with S2B dissociated from either Fe2 or Fe6 (S2F, S2S, S6M, S6S, S6M2 and S6S2, named the same way as for the E_3 structures, as is described in Table 6 and shown in Fig. 7; the two structures with a final "2" have the proton on S5A pointing towards S2B rather than towards S3A). Finally, we studied one structure with a proton on S2B and hydride ions on Fe5, Fe6 and bridging Fe2/6 (called 3H)[37] and one structure with a proton on S2B and the central carbide ion triply protonated (C3).[37]

Table 5 Structures studied for the E_3 state with N_2. The structures are the same as in Table 4 and the entries are the same as in Table 3. All Fe–N bond lengths are in Å (a distance in bold face indicates a restrained bond) and all energies in kJ mol⁻¹. The structures were studied in the BS10-147 state, unless otherwise stated.

		TPSS						r2SCAN				TPSSh				B3LYP			
		Fe–N	ΔE	ΔE_{N_2}	ΔE_{db}	FeN$_{TS}$	ΔE_{TS}	Fe–N	ΔE	ΔE_{N_2}	ΔE_{db}	Fe–N	ΔE	ΔE_{N_2}	ΔE_{db}	Fe–N	ΔE	ΔE_{N_2}	ΔE_{db}
F2 + N2	345	2.91[a]	112.9	67.4				2.75	84.0	93.2		2.69	75.8	78.6		2.66	58.5	266.3	
	335	**2.80**	119.1	73.5				**2.80**	92.5	101.6		**2.80**	72.8	75.5		**2.80**	89.2	297.0	
	355	2.84[a]	119.5	74.0				2.54	83.5	92.7		2.63	65.7	68.4		2.66	57.7	265.5	
	35_2	2.75	123.9	78.3				2.02	62.3	71.5		2.70	67.0	69.8		2.61	23.5	231.3	
	35_3	**2.80**	110.9	65.4				**2.80**	64.0	73.1		**2.80**	54.0	56.8		**2.80**	16.6	224.4	
	352_	**2.80**	114.3	68.8				**2.80**	94.8	104.0		**2.80**	85.5	88.3		**2.80**	98.6	306.4	
	S6M	**2.80**	58.6	13.1				**2.80**	31.0	40.2		**2.80**	18.6	21.4		**2.80**	−7.3	200.5	
	S6S	**2.80**[b]	58.2	12.6				**2.80**[c]	47.5	56.7		**2.80**[c]	9.6	12.3		**2.80**	−17.9	189.9	
	C3	**2.80**	250.8	205.3				**2.80**[c]	156.7	165.9		**2.80**[c]	34.8	37.6		**2.80**[c]	−180.2	27.6	
Fe6 + N2	345	3.67	103.6	58.1				3.71	50.0	59.2		3.72	60.3	63.0		3.72	44.8	252.6	
	335	3.65	75.7	30.1				3.78	71.8	81.0		3.76	56.8	59.6		3.79	77.4	285.2	
	355	3.70	97.5	52.0				3.65	64.4	73.6		3.74	68.1	70.9		3.72	74.4	282.2	
	35_2	3.69	92.6	47.0				3.70	50.3	59.5		3.77	36.8	39.6		3.83	−6.9	200.9	
	35_3	3.72	82.9	37.4				3.69	39.2	48.4		3.74	25.7	28.4		3.74	−14.6	193.2	
	352_	3.62	96.9	51.4				3.58	73.0	82.2		3.61	69.2	72.0		3.62	65.5	273.3	
	S2F	**2.80**	63.2	17.6				**2.80**	21.6	30.8		**2.80**	11.6	14.3		**2.80**	25.7	233.5	
	S2S	**2.80**[b]	74.1	28.6				**2.80**[d]	98.6	107.8		**2.80**[d]	72.8	75.5		**2.80**	148.2	355.9	
	C3	**3.70**	337.1	291.6				**3.70**	235.6	244.8		**3.70**	131.2	134.0		**3.70**	−104.1	103.7	
Fe2 – N2	345	1.91	116.5	70.9	3.5	No barrier		2.02	87.4	96.5	3.4	1.91	145.3	148.1	69.5	1.89	135.5	343.3	77.0
	335	1.94	99.3	53.8	−19.8	No barrier		2.03	76.4	85.5	−7.1	2.09	68.5	71.3	−4.2	2.34	67.2	275.0	−22.0
	355	1.93	91.8	46.3	−27.7	2.4	4.5	1.93	61.8	71.0	−0.5	2.08	63.6	66.4	−2.0	2.31	80.9	288.7	23.2
	35_2	1.89	86.7	41.2	−37.1	No barrier		1.93	48.2	57.3	−15.8	1.97	52.7	55.4	−14.4	2.13	23.1	230.8	−0.4
	35_3	1.90	78.4	32.9	−32.5	No barrier		1.88	79.4	88.5	−15.5	1.97	28.0	30.7	−26.1	2.14	9.1	216.9	−7.5
	352_	1.85	73.9	28.4	−40.4	No barrier		1.84	0.4	9.6	−30.6	1.88	69.4	72.2	−16.1	1.90	88.9	296.7	−9.7
	S6M	1.85[b]	22.9	−22.6	−35.7	No barrier		1.84	0.0	9.2	−47.5	1.84	0.0	2.8	−18.6	2.36	1.1	208.9	8.4
	S6S	1.83[b]	15.8	−29.8	−42.4							1.84	1.1	3.9	−8.4	1.88	0.0	207.8	17.9
	C3	1.78[c]	227.4	181.9	−16.9		34.7	1.76[c]	154.1	163.3	1.3	1.88	56.8	59.5	36.2	2.28	−179.7	28.1	0.5
Fe6 – N2	345	1.81	130.0	84.5	26.4	2.1		1.80	71.9	81.0	0.1	1.87	120.5	123.3	60.2	1.90	120.3	328.1	75.5
	335	1.81	66.1	20.6	−9.5	2.3	19.1	1.80	76.2	85.4	11.8	1.83	51.9	54.7	−4.9	1.86	81.4	289.2	4.0
	355	1.81	87.2	41.7	−11.9	2.3	12.0	1.90	96.3	105.4	0.0	1.82	59.5	62.3	−8.6	1.85	88.3	296.1	13.9
	35_2	**1.90**[b]	100.5	54.9	7.9			**1.90**	96.3	105.4	0.0	**1.90**[b]	67.9	70.7	31.1	**1.90**[b]	121.4	329.1	128.3
	35_3	1.85	89.4	43.9	6.5	2.3	18.4	1.85	142.5	151.7	54.8	1.87	69.0	71.8	43.4	1.93	95.5	303.3	110.1
	352_	1.83	120.2	74.7	23.3	2.3	27.4	1.83	36.8	46.0	69.5	1.84	117.0	119.7	47.8	1.90	173.3	381.1	107.8
	S2F	1.79[b]	14.4	−31.2	−48.8	No barrier		1.86	29.8	39.0	15.2	1.80[b]	31.6	34.4	20.0	2.41	27.2	235.0	1.5
	S2S	1.80[b]	0.0	−45.5	−74.1	No barrier		1.79[b]	101.6	110.8	−68.8	1.81[b]	20.9	23.7	−51.8	2.31	27.2	235.0	−121.0
	C3	1.73[e]	186.0	140.4	−4.8			1.96[c]			−134.1	1.76	52.4	55.2	−78.8	1.80	−163.6	44.2	−44.8

[a] Studied in the BS7-235 state. [b] Studied in the BS-14 state. [c] Studied in the BS10-136 state. [d] Studied in the BS10-146 state. [e] Studied in the BS8-245 state.
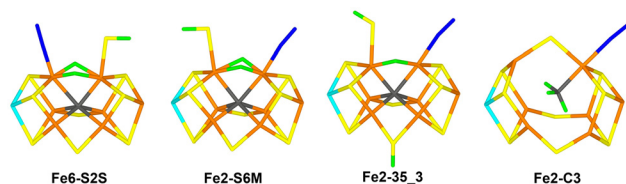
Fig. 6 The best E_3 structures with N_2 bound, Fe6-S2S, Fe2-S6M, Fe2-35_3 and Fe2–C3. The first three structures were optimised with TPSS, whereas Fe2–C3 was optimised with B3LYP.

The relative stability of the various E_4 states without any N_2 are shown in Table 6. The S6S structure (with two hydride ions bridging Fe2/6 and the protonated S2B dissociated from Fe2; Fig. 7) is most stable with TPSS, r^2SCAN and TPSSh. However, with TPSS, eight structures are within 15 kJ mol^{-1}. Three of these, S6M, 3323 and 3523 (Fig. 7), are within 25–29 and 11–18 kJ mol^{-1} of S6S for r^2SCAN and TPSSh, respectively. Changing the proton on S5A in the S6S structure so that it points towards S2B instead of S3A decreases the stability by 9–13 kJ mol^{-1}. Likewise, dissociating S2B from either Fe2 or Fe6 in the 3323 or 3523 structures also makes the structures less stable. With B3LYP, instead the structure with a triply protonated carbide ion (C3; Fig. 7) is by far the best, 192 and 229 kJ mol^{-1} more stable than 3523 and S6S, respectively. With TPSSh, the C3 structure is only 1 kJ mol^{-1} less stable than S6S, whereas it is 146–192 kJ mol^{-1} less stable than the best structure for the other two functionals. Thus, the E_4 state remains a challenge for computational methods in that several

structures are close in energy and the preferred structure depends strongly on the DFT functional.

For the best structures, we studied the binding of N_2. The results are shown in Table 7. N_2-bound structures were found for all structures studied and both Fe ions, except Fe6-3323H2 and Fe6-5522 with B3LYP. For all four functionals, S2B dissociates spontaneously from Fe2 when N_2 binds to this ion for all structures with the Fe2/6 hydride on the S3A side (with B3LYP also the 3322 and 3522 structures). In principle, such half-dissociation of S2B should remove the dependency on the conformations of the H atoms on S2B and Fe2/6. However, in practice there are still distinct local minima for both H atoms (for example, the hydride bridging Fe2/6 can still bend towards S3A or towards S5A, although S2B is no longer in between the two conformations), but the barriers between them are most likely appreciably lower. S2B does not dissociate spontaneously when N_2 binds to Fe6, but half-dissociated structures with N_2 bound are typically lower in energy for the cases we have tested.

With TPSS, the S2S structure with N_2 bound to Fe6 is most stable (Fig. 8). It gives a Fe6–N distance of 1.79 Å and a favourable ΔE_{N_2} binding energy of −51 kJ mol^{-1}. The S6S and 3523 structures with N_2 binding to Fe2 are 9 and 32 kJ mol^{-1} less stable, respectively (Fig. 8). With r^2SCAN, instead Fe2-S6S is most stable, with Fe–N = 1.79 Å and ΔE_{N_2} = −44 kJ mol^{-1}. The Fe6-S2S structure is 11 kJ mol^{-1} less stable. With TPSSh, the same structures are also among the best ones and degenerate within 0.2 kJ mol^{-1}. However, the Fe6–C3 structure (Fig. 8) is actually 1 kJ mol^{-1} more stable. It has Fe–N bond length of 1.83 Å and ΔE_{N_2} = −27 kJ mol^{-1}. With B3LYP, the Fe2–C3 struc-

Table 6 The 20 structures studied for the E_4 state without N_2. ΔE is the relative energy for each DFT method (kJ mol^{-1}). The H1, H2, H3 and H4 columns describe positions and directions of the four H atoms. The nomenclature is the same as in Table 2. The structures were studied in the BS10-147 state, unless otherwise stated.

| | H1 | H2 | H3 | H4 | ΔE | | | |
					TPSS	r2SCAN	TPSSh	B3LYP
3H	S2B(3)	Fe2/6(3)	Fe5	Fe6	40.3[a]	125.0	112.0	141.2
3322	S2B(3)	Fe2/6(3)	Fe3/7(2)	S5A(2)	15.1	52.5	38.6	100.5
3323	S2B(3)	Fe2/6(3)	Fe3/7(2)	S5A(3)	3.2[a]	27.4[b]	11.3[b]	41.5[b]
3323H2	S2B(H2F)	Fe2/6(3)	Fe3/7(2)	S5A(3)	118.0[a]	79.3	102.6	202.9
3323H6	S2B(H6S)	Fe2/6(3)	Fe3/7(2)	S5A(3)	39.0	43.5	49.2	121.6
3522	S2B(3)	Fe2/6(5)	Fe3/7(2)	S5A(2)	24.0	76.2[a]	48.0[a]	74.7
3523	S2B(3)	Fe2/6(5)	Fe3/7(2)	S5A(3)	14.0[a]	25.4	17.9[b]	0.0[c]
3523H2	S2B(H2F)	Fe2/6(5)	Fe3/7(2)	S5A(3)	114.9			203.0
3523H6	S2B(H6S)	Fe2/6(5)	Fe3/7(2)	S5A(3)	39.3	43.7	49.2	101.8
5322	S2B(5)	Fe2/6(3)	Fe3/7(2)	S5A(2)	21.7[a]	59.0	48.1	113.9
5323	S2B(5)	Fe2/6(3)	Fe3/7(2)	S5A(3)	11.1[a]	45.0	37.0	104.1
5522	S2B(5)	Fe2/6(5)	Fe3/7(2)	S5A(2)	40.6[a]	59.0	51.3	113.8
5523	S2B(5)	Fe2/6(5)	Fe3/7(2)	S5A(3)	29.7[a]	43.2	40.4	104.7
S2F	S2B(H2F)	Fe2/6(3)	Fe2/6(5)	S5A(3)	54.1	78.7	56.2	101.3
S2S	S2B(H2S)	Fe2/6(3)	Fe2/6(5)	S5A(3)	54.8	76.4	56.4	108.2
S6M	S2B(H6M)	Fe2/6(3)	Fe2/6(5)	S5A(3)	0.6	28.5	18.1	65.5
S6S	S2B(H6S)	Fe2/6(3)	Fe2/6(5)	S5A(3)	0.0	0.0[c]	0.0[d]	37.0[e]
S6M2	S2B(H6M)	Fe2/6(3)	Fe2/6(5)	S5A(2)	10.1	39.8	25.5	76.4
S6S2	S2B(H6S)	Fe2/6(3)	Fe2/6(5)	S5A(2)	9.4	38.3	29.6	64.5
C3	S2B(3)	C2367	C2456	C3457	191.7[f]	145.9[c]	1.3[f]	−191.5[f]

[a] Studied in the BS-14 state. [b] Studied in the BS10-135 state. [c] Studied in the BS7-346 state. [d] Studied in the BS6-157 state. [e] Studied in the BS8-347 state. [f] Studied in the BS2-234 state.
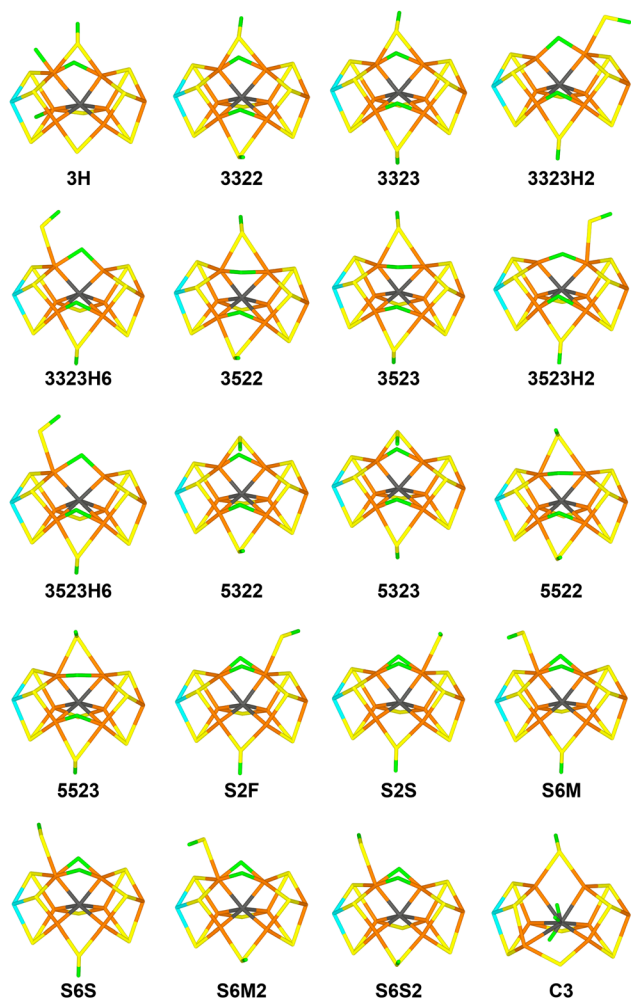
Fig. 7 The 20 E_4 structures without N_2 bound. The positions of the added H atoms are described in Table 6 and the nomenclature is explained in the text.

ture is the most stable, 46 kJ mol^{-1} better than Fe6–C3 and 225 kJ mol^{-1} better than Fe2-S6S. It has a Fe–N bond length of 2.18 Å and the ΔE_{N_2} binding energy is −13 kJ mol^{-1}.

With TPSS, we could find structures with N_2 residing in the second coordination sphere of Fe2 or Fe6 for all the Hoffman-type and 3H structures, but not for the structures with S2B half-dissociated or the C3 structures. With the other functionals, the same applied for N_2 binding in the second sphere of Fe6, but for Fe2, second-sphere structures were found only for 3H, 5322 and 5323 (also 3322 and 3323 with r^{2}SCAN and TPSSh). The Fe6-3323 structure is the best for TPSS and TPSSh, whereas Fe6-3523 is best with r^{2}SCAN, and Fe6-3522 is best for B3LYP. In all cases, the structures with N_2 in the second sphere are appreciably less stable than those with N_2 binding in the first sphere, by at least 59, 50, 51 and 274 kJ mol^{-1} for TPSS, r^{2}SCAN, TPSSh and B3LYP, respectively. Therefore, the barriers for N_2 binding to Fe2 are all low, below 14 kJ mol^{-1} and often barrierless. For the binding to Fe6, the barriers are higher, 15–39 kJ mol^{-1}, but 79 kJ mol^{-1} for the 3H structure.

Discussion

The prime results in this investigation are the binding energies. Unfortunately, they depend on the DFT functional and on how it is defined. We argue that it is most reasonable to use the QM/MM energy of the best structure of the same E_n state and free N_2 in a water-like continuum solvent as the reference (ΔE_{N_2}). For most functionals, this gives binding energies of the most stable N_2-bound structures that become increasingly negative (favourable) when going from E_0 to E_4 (employing restraints to obtain a bound state if no such state is found): 34, 26, −11, −46 and −51 kJ mol^{-1} for TPSS, 57, 41, 15, 9 and −44 kJ mol^{-1} for r^{2}SCAN, 58, 50, 9, 3 and −27 kJ mol^{-1} for TPSSh, and 41, 74, 22, 28 and −6 kJ mol^{-1} for B3LYP (somewhat less regular). As mentioned in the Method section, it is likely that the def2-SV(P) basis set give ΔE_{N_2} binding energies that are ~14 kJ mol^{-1} too negative (too favourable, *cf.* Table S3†), so we will in the following discussion add 14 kJ mol^{-1} to the ΔE_{N_2} energies.

As mentioned in the Introduction, Bjornsson and co-workers report more favourable binding energies, based on TPSSh calculations, −29 kJ mol^{-1} for E_2 (Fe6-H$_2$S) and −43 or −56 kJ mol^{-1} for E_4 (Fe2–H6 or Fe6–H2).[52] The reason for this is mainly that he uses another definition for the binding energy (ΔE_{bn} in eqn (4)). With this definition, we obtain ΔE_{bn} = −43 kJ mol^{-1} for E_2-Fe6-H$_2$S and −82 kJ mol^{-1} for E_4-Fe6-H$_2$S (because the H$_2$S is not the best structure neither for E_2 nor for E_4). Likewise, Dance obtains more favourable binding energies[59] than we do because he uses the ΔE_{db} definition in eqn (3). Moreover, all his E_4 structures involve a bound H$_2$ molecule, *i.e.* a type of structures not included in our investigation.

It should be noted that binding energies discussed so far are pure (electronic) energies. To compare with experimental results, we need to use free energies, *i.e.* to add enthalpic and entropic corrections. In particular, N_2 loses translational and rotational entropy upon binding. Unfortunately, there is no consensus in the size of this entropic penalty. Bjornsson and coworkers, as well as Siegbahn, use DFT frequency calculations to estimate an entropic penalty of 41–45 kJ mol^{-1}.[52,60,61] On the other hand, Dance argues that the relevant dissociated state is N_2 at a diffusible position inside the protein, where it has already lost most of its translational and rotational entropy. Therefore, he suggests a much smaller entropic penalty of ~17 kJ mol^{-1}.[58]

With the entropy correction of Bjornsson and Siegbahn, together with the basis-set correction, none of the DFT methods give favourable N_2 binding for any of the E_n states, although for E_4 with TPSS, ΔE_{N_2} is only slightly positive (~6 kJ mol^{-1}). With Dance's entropy penalty (and the basis-set correction), TPSS suggests that N_2 cannot bind to E_0–E_2, but that it binds to E_3 and E_4, in accordance with the experimental data.[1,25,28–30] B3LYP and TPSSh still give no favourable N_2 binding to any E_n state (although that to E_4 for TPSSh is only slightly positive, by 4 kJ mol^{-1}). For r^{2}SCAN, ΔE_{N_2} is favourable to E_4 (by 13 kJ mol^{-1}) and unfavourable to the other states.

Table 7 Structures studied for the E_4 state with N_2. The structures are the same as in Table 4 and the entries are the same as in Table 3. All Fe–N bond lengths are in Å (a distance in bold face indicates a restrained bond) and all energies in kJ mol^{-1}. The structures were studied in the BS-14 state, unless otherwise stated.

		TPSS						r2SCAN				TPSSh				B3LYP			
	Structure	Fe–N	ΔE	ΔE_{N_2}	ΔE_{db}	FeN$_{TS}$	ΔE_{TS}	Fe–N	ΔE	ΔE_{N_2}	ΔE_{db}	Fe–N	ΔE	ΔE_{N_2}	ΔE_{db}	Fe–N	ΔE	ΔE_{N_2}	ΔE_{db}
Fe2 + N_2	3H[a]	2.97	87.3	36.5				3.12	119.0	100.5		3.06	124.0	97.2		3.08	174.9	393.9	
	3322	2.85	95.9	45.1				2.90[b]	102.7	84.1		2.80[b]	95.1	68.2					
	3323	2.77	86.8	36.0				2.79	117.3	98.7		2.71	95.0	68.1					
	3323H6[b]	2.80	115.1	64.2				2.80	93.1	74.5		2.80	85.2	58.4		2.80	83.7	302.7	
	3522	2.68	112.0	61.1				2.80	80.3	61.8		2.80[f]	85.7	58.9		2.80[d]	15.3	234.4	
	5523	1.87	59.8	8.9															
	5523H6[b]	2.80	102.2	51.4				2.80	104.8	86.3		2.80	90.4	63.6		2.80	91.3	310.3	
	5322	2.82	93.5	42.7				3.02[b]	104.0	85.5		2.88[b]	96.5	69.6		2.85[b]	108.0	327.0	
	5323[b]	2.79	59.8	34.4				2.96	91.6	73.0		2.88	84.3	57.5		2.78	85.6	304.7	
	5522	2.70	127.6	76.8															
	5523	2.71	120.6	69.8															
	S6M[b]	2.80	70.0	19.1				2.80	68.7	50.1		2.80	60.6	33.8		2.80	−8.3	210.7	
	S6S	2.80[c]	75.7	24.9				2.80[c]	47.0	28.5		2.80[d]	26.7	−0.1		2.80[e]	−6.6	212.4	
	S6M2[b]	2.80	78.9	28.0				2.80	108.9	90.3		2.80	74.5	47.6		2.80	99.4	318.5	
	C3	2.80[e]	322.7	271.8				2.80	198.8	180.2		2.80[f]	28.5	1.7		2.80[a]	−157.2	61.9	
Fe6 + N_2	3H[a]	3.79	72.1	21.2				3.81	91.7	73.2	15.5	3.85	100.5	73.7		3.77	147.6	366.6	
	3322	3.69	70.2	19.4				3.72[b]	67.5	48.9	−22.7	3.72[b]	70.0	43.1		3.80[b]	54.7	273.7	
	3323	3.72	59.0	8.1				3.70[b]	51.9	33.4	−25.2	3.71[b]	51.2	24.3		3.74[b]	67.0	286.1	
	3323H6[b]	3.57	82.2	31.3				3.56[b]	65.5	47.0	−26.5	3.60[b]	68.1	41.3		3.58[b]	48.3	267.3	
	3522	3.57	72.7	21.8				3.57[b]	50.0	31.5	−33.0	3.60[b]	58.2	31.4		3.60[b]	69.6	288.7	
	5523	3.16	68.5	17.6				3.32	102.0	83.4	−70.5	3.24[b]	76.8	50.0		3.50[b]	64.0	283.0	
	5523H6[b]	3.19	60.5	9.6				3.33[b]	63.0	44.4	−9.6	3.24	65.3	38.4		3.75[b]	59.0	278.0	
	5322	3.56	98.7	47.9				3.55	115.0	96.5	−23.9	3.58	103.3	76.5		3.53[b]	91.8	310.8	
	5323	3.54	87.6	36.7				3.52[b]	63.5	45.0	−68.5	3.55[b]	75.5	48.7		3.50[b]	51.5	270.5	
	S2F[b]	2.80	80.6	29.7				2.80[e]	64.2	45.7	−72.5	2.80	60.1	33.3		2.80[e]	14.6	233.6	
	S2S[b]	2.80	80.7	29.9				2.80	68.5	50.0	−40.2	2.80	65.1	38.3		2.80	62.3	281.3	
	C3[a]	3.70	246.2	195.3				3.70	142.5	123.9	−47.0	3.70	29.9	3.1		3.70	−212.2	6.8	
Fe2–N_2	3H[a]	1.83	76.9	26.0	−10.4	2.5	14.0	1.86	134.5	116.0	15.5	1.84	130.0	103.2	6.0	1.87	182.2	401.2	7.3
	3322	1.89	67.2	16.3	−28.7	2.6	0.1	1.90	105.0	86.5		1.91[b]	81.6	54.7	−22.8	1.97[b]	80.4	299.4	−60.6
	3323	1.89	56.6	5.7	−30.2	2.6	0.8	1.90[b]	92.0	73.5		1.90[b]	81.3	54.5	−13.6	1.96[b]	75.3	294.3	−55.1
	3323H6[b]	1.84	57.6	6.8	−57.4	No barrier		1.86	66.6	48.0		1.86	48.3	21.5	−36.9	1.87	53.2	272.2	−30.6
	3522	1.84[b]	49.1	−1.8	−62.9	No barrier		1.96[g]	62.8	44.3		1.87[b]	53.8	27.0	−24.5	2.12[g]	46.8	265.8	7.6
	5523	1.83[c]	32.0	−18.8	−73.7	2.6	1.4	1.98[d]	47.4	28.8		1.89[a]	29.6	2.8	−56.1	2.29[a]	22.9	241.9	−32.8
	5523H6[b]	1.84	40.4	−10.5	−61.9	2.5	2.4	1.86	57.7	39.1		1.87	42.7	15.9	−47.7	1.90	58.5	277.5	−44.5
	5322	1.87	70.8	19.9	−22.7	2.5	1.7	1.87[b]	107.8	89.3		1.89[b]	75.6	48.7	−29.8	1.93[b]	109.5	328.5	−46.0
	5323	1.88	60.2	9.3	−25.1	2.5	0.1	1.87[b]	93.5	75.0		1.89[b]	62.1	35.3	−33.0	1.93[b]	97.3	316.4	−105.1
	5522[b]	1.83	66.3	15.5	−61.3	No barrier		1.85	84.9	66.4		1.86	68.4	41.5	−2.4	1.88	62.5	281.6	−106.9
	5523	1.83	57.1	6.2	−63.6	No barrier		1.85[b]	72.6	54.1		1.86	56.4	29.6	−3.4	1.88[b]	53.0	272.0	62.5
	S6M	1.84	34.2	−16.7	−35.8	No barrier		1.84[b]	28.5	9.9		2.19[b]	54.8	27.9	−5.9	2.36[b]	54.1	273.2	6.6
	S6S	1.83[b]	9.4	−41.5	−66.3	No barrier		1.79[c]	0.0	−18.5		1.84[c]	1.2	−25.6	−25.5	1.87[c]	0.0	219.0	−63.8
	S6M2	1.83	44.9	−6.0	−33.9	No barrier		1.84[b]	41.5	23.0		1.85[b]	41.1	14.3	−33.4	1.88[b]	35.6	254.6	−21.7
	C3[a]	1.88[a]	202.3	151.4	−120.4			1.77[e]	67.7	49.2		1.81[d]	21.8	−5.0		2.18[a]	−178.9	40.1	
Fe6–N_2	3H[a]	1.80	123.6	72.7	51.5	2.2	79.2	1.79	143.8	125.2	52.0	1.82	149.6	122.7	49.0	1.86	190.9	409.9	43.3
	3322	1.82[g]	72.0	21.1	1.8	2.3	29.4	1.83[g]	112.5	93.9	17.5	1.85[g]	99.6	72.7	20.9	1.87	143.8	362.8	20.6
	3323	1.80[a]	52.6	1.7	−6.4	2.3	31.1	1.79[h]	73.6	55.1	25.6	1.93[e]	48.3	54.5	33.0	1.89[a]	98.1	317.1	58.5
	3323H2	1.82	56.2	5.3				1.85	96.0	77.5		1.88	75.4	48.6					
	3522	1.82	101.4	50.5	19.2	2.2	39.0	1.81	138.2	119.6	39.0	1.84	118.1	91.3	33.0	1.94	158.5	377.5	25.3
	3523	1.82	91.8	41.0	19.2	2.2	38.1	1.81	126.3	107.8	76.3	1.84	108.2	81.3	49.9	1.84	150.6	369.6	26.6

Table 7 *(Contd.)*

	TPSS						r2SCAN				TPSSh				B3LYP			
	Fe–N	ΔE	ΔE_{N_2}	ΔE_{db}	FeN$_{TS}$	ΔE_{TS}	Fe–N	ΔE	ΔE_{N_2}	ΔE_{db}	Fe–N	ΔE	ΔE_{N_2}	ΔE_{db}	Fe–N	ΔE	ΔE_{N_2}	ΔE_{db}
3523H2	1.79	58.3	7.5	0.0	2.3	21.1	1.85[g]	65.8	47.3	−0.8	1.81[b]	52.0	25.2	0.1	2.28[b]	96.5	315.6	−66.7
5322	1.84	71.8	21.0	3.3	2.3	21.0	1.81[b]	101.2	82.7	−12.7	1.99	86.2	59.4	−0.2	3.25[b]	63.8	282.8	−66.6
5323	1.84	63.5	12.6	3.0	2.2	26.5	2.05[b]	79.2	60.7	15.7	1.99	76.1	49.3	13.8	3.25[b]	52.6	271.7	
5522	1.83	94.2	43.3	−4.5	2.2	25.8	1.92	130.7	112.2	−46.8	1.90	117.1	90.3	−46.5	1.91	146.4	365.4	6.7
5523	1.83	83.2	32.3	−4.4	2.4	14.9	2.03[b]	90.0	71.4	−31.1	2.11[b]	89.9	63.1	−25.2	1.86[b]	67.0	286.0	27.9
S2F	1.79	15.7	−35.2	−64.9	No barrier		1.81[b]	41.9	23.4	−57.8	1.81[b]	34.9	8.0	−63.7	1.84[e]	41.3	260.3	−21.0
S2S	1.79[c]	0.0	−50.9	−80.7			1.79[a]	10.7	−7.8	−33.0	1.80[a]	1.4	−25.4	−29.9	2.18[a]	−225.3	−6.2	−13.0
C3	1.74[a]	201.7	163.1	5.6			1.84[f]	109.5	90.9		1.83	0.0	−26.8					

[a] Studied in the BS2-234 state. [b] Studied in the BS10-147 state. [c] Studied in the BS10-146 state. [d] Studied in the BS6-157 state. [e] Studied in the BS10-135 state. [f] Studied in the BS8-347 state. [g] Studied in the BS7-235 state. [h] Studied in the BS7-346 state.
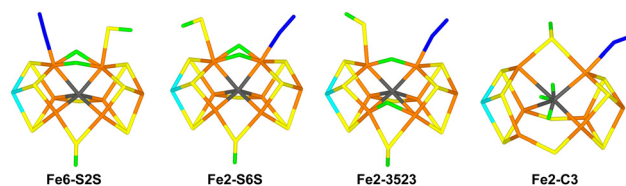
Fig. 8 The best E_4 structures with N_2 bound, Fe6-S2S, Fe2-S6S, Fe2-3523 and Fe2–C3. The first three structures were optimised with TPSS, whereas Fe2–C3 was optimised with B3LYP.

These results can be interpreted in several ways. One interpretation is that TPSS is the only DFT method that gives reasonable binding energies. This is the most direct interpretation of the results, but it is weakened by the fact that TPSSh and r^{2}SCAN give better geometries of the FeMo cluster[83] and that TPSS typically does not give the most accurate energies, neither for main-group molecules,[101] nor for nitrogenase-type reactions[102,103] (but for hydrogenase models, TPSS has been shown to give more accurate results than B3LYP[104,105]).

As already discussed, there are different definitions of the binding energy. ΔE_{N_2} has the advantage of using well-defined states and the most stable structures for both the bound and unbound states. However, it is sensitive to that we really find the best possible structures, as well as spin and BS state of the two structures, which is a formidable task. The direct binding energy, ΔE_{db} in eqn (3) is typically more favourable (negative) than ΔE_{N_2}, mainly because it is not based on the most stable structure for the unbound state. Unfortunately, owing to the non-polar nature of N_2, the unbound complexes are weak and therefore rather poorly defined and quite often the binding is barrierless, so that no unbound structure of the same type is found. Then ΔE_{db} is undefined or has to be based on a structure with a restrained Fe–N distance. Our calculations are based on the philosophy that the relevant states involved in the reaction mechanism are those with the lowest energies (less stable state should have minor populations under normal conditions, unless they are strongly kinetically favoured). However, if we consider the best bound state and use restrained structures when no unbound state is found, we get ΔE_{db} energies of 33, 24, −34, −74 and −81 kJ mol^{-1} for TPSS, 61, 4, −7, −48 and −47 kJ mol^{-1} for r^{2}SCAN, 56, 14, −13, −19 and −30 kJ mol^{-1} for TPSSh and 44, 74, 10, 0 and −13 kJ mol^{-1} for B3LYP for the E_0–E_4 states. Thus, with the basis-set and entropy corrections, no state is bound for B3LYP and TPSSh, E_3 and E_4 are bound with TPSS, whereas whether E_2 is bound with TPSS, E_3 and E_4 are bound with r^{2}SCAN depends on the size of the entropy correction (*i.e.* bound with Dance's penalty, but not with that of Bjornsson or Siegbahn).

A third interpretation is that N_2 actually does not bind directly to E_4 (or E_3). In fact, it has been suggested that formation of H_2 by reductive elimination is a necessary requisite for the binding of N_2.[54,55] In particular, H_2 should be formed by a reaction between the two hydride ions in E_4 and it has been suggested that thereby a reactive state of E_2 is formed

with two protonated sulfide ions, *i.e.* a state in which the FeMo cluster is formally two steps more reduced than the most stable E_2 state with one proton and one hydride ion (if H on sulfide is considered as a proton and H on Fe as a hydride ion, the two states would formally be $Fe_5^{II}Fe_2^{III}H_2^+$ and $Fe_3^{II}Fe_4^{III}H^+H^-$). However, Dance has argued that this is not supported by QM calculations, showing only minor differences between H atoms on S or Fe[35,106] and calculations of redox potentials support the latter view.[107] The results in Table 2 shows that the best structure with two protons on sulfide ions (N33) is 11–55 kJ mol^{-1} less stable than the most stable E_2 structures with the four DFT methods. Moreover, neither N33 nor the N25 structure shows any enhanced N_2 binding energies (Table 3), irrespectively if using the ΔE_{N_2} (40–67 kJ mol^{-1}, compared to −11 kJ mol^{-1} for Fe6–B33, B35 and H2F with TPSS) or the ΔE_{db} definition (−6 to +11 kJ mol^{-1}, compared to −29 to −76 kJ mol^{-1} Fe6–B33, B35 and H2F with TPSS; qualitatively similar results are obtained also with the other functionals). In a future study, we will study the dissociation of H_2 from the various E_n states, whether N_2 may bind concomitantly with the dissociation of H_2 from E_4 or if a bound H_2 molecule may enhance the binding of N_2.

A fourth possible interpretation of the poor binding with hybrid DFT functionals has been given by Siegbahn, who has suggested that the FeMo cluster needs to be reduced by four more electrons before N_2 may bind favourably.[60,61] This is an interesting suggestion, but the need of such additional reduction steps is not supported by experimental data.[3,4]

Our results are quite similar to those found in other studies. For example, the recent study by Pang and Bjornsson reports N_2 binding energies (calculated with the r^{2}SCAN functional) of 69, 41, 8 and −17 kJ mol^{-1} to the E_0, E_1, E_2 and E_4 states, respectively,[53] which are similar to our results 57, 41, 15 and −44 kJ mol^{-1}. Our suggestions of the most stable states with or without N_2 bound also reasonably agree, but we find a smaller energy difference (still with the r^{2}SCAN functional) between the best H6S or S6S structures for the E_2 and E_4 states without N_2 and alternative structures B35 (17 kJ mol^{-1}) or 3523/3323 (25–27 compared to 70–73 kJ mol^{-1}) and also a preference for N_2 binding to Fe2 rather than Fe6. The differences are understandable considering the differences in details of the calculations and the many possible BS states and conformations for the added protons.

Conclusions

In this work, we have studied the binding of N_2 to the E_0–E_4 states of Mo-nitrogenase with four different DFT methods. This has given a number of interesting and useful results.

• We provide further information about the stability of various structures of the E_3 and E_4 states. We show that S6M and S6S states (with two hydride ions both bridging Fe2/6 and with a protonated S2B ligand dissociated from Fe2) are the best models for the E_3 state with the TPSS, TPSSh and r^{2}SCAN functionals, but with B3LYP a triply deprotonated carbide ion

is much more stable (and this state is only 4 kJ mol^{-1} less stable than the best by TPSSh). For the E_4 state, the situation is slightly more complicated. Because several structures have comparable energies: With the TPSS, TPSSh and r^{2}SCAN functionals, the S6S structure is most stable, but the 3323 and 3523 structures are within 3–27 kJ mol^{-1}. The C3 structure is best for B3LYP and degenerate with S6S for TPSSh.

• Binding of N_2 is observed for the E_2–E_4 states. It binds end-on in the exo position (*i.e. trans* to the central carbide) to either Fe2 or Fe6. Typical Fe–N bond lengths are 1.80–1.98 Å.

• Half-dissociation of S2B enhances the binding of N_2, especially to Fe2. As observed before for the E_2 state,[63] the preference for half-dissociation is lower with the TPSS functional, than with the other functionals.

• TPSS consistently favours binding of N_2 to Fe6, whereas the other three functionals mostly prefer binding to Fe2.

• The binding free energy depends on the DFT functional, the entropy correction and on how the binding is defined. With the large entropy correction of Bjornsson and Siegbahn (41–45 kJ mol^{-1}), no functional gives favourable binding to any E_n state. Using the QM/MM energy of the best structure of the same E_n state and free N_2 in a water-like continuum solvent as the reference (ΔE_{N_2}) and Dance's lower entropy penalty (17 kJ mol^{-1}), TPSS gives favourable binding to the E_3 and E_4 states and r^{2}SCAN only to E_4. B3LYP and TPSSh still give no favourable N_2 binding to any E_n state.

Thus, our results show that computational results for the N_2 binding to the FeMo cluster strongly depends on the DFT method employed, with hybrid functionals giving a weaker binding, favouring binding to Fe2 and protonation of the central carbide. However, it is likely that structures with the S2B ligand dissociated from either Fe2 or Fe6, as well as structures with two hydride ions both bridging Fe2 and Fe6 are involved in the reaction mechanism. On the other hand, we find no support to the suggestion that reductive elimination of the two hydride ions in E_4 would enhance the binding of N_2. Clearly, further studies of the dissociation of H_2 from the FeMo cluster and how it affects the binding of N_2 are needed.

Conflicts of interest

There are no conflicts to declare.

Acknowledgements

References

1 B. K. Burgess and D. J. Lowe, *Chem. Rev.*, 1996, **96**, 2983–3012.

2 B. Schmid, H.-J. Chiu, V. Ramakrishnan, J. B. Howard and D. C. Rees, *Handbook of Metalloproteins*, John Wiley & Sons, Ltd, 2006, pp. 1025–1036, DOI: 10.1002/0470028637.met174.

3 B. M. Hoffman, D. Lukoyanov, Z.-Y. Yang, D. R. Dean and L. C. Seefeldt, *Chem. Rev.*, 2014, **114**, 4041–4062.

4 L. C. Seefeldt, Z.-Y. Yang, D. A. Lukoyanov, D. F. Harris, D. R. Dean, S. Raugei and B. M. Hoffman, *Chem. Rev.*, 2020, **120**, 5082–5106.

5 J. Kim and D. C. Rees, *Science*, 1992, **257**, 1677–1682.

6 O. Einsle, F. A. Tezcan, S. L. A. Andrade, B. Schmid, M. Yoshida, J. B. Howard and D. C. Rees, *Science*, 2002, **297**, 1696–1696.

7 T. Spatzal, M. Aksoyoglu, L. Zhang, S. L. A. Andrade, E. Schleicher, S. Weber, D. C. Rees and O. Einsle, *Science*, 2011, **334**, 940–940.

8 T. Spatzal, K. A. Perez, O. Einsle, J. B. Howard and D. C. Rees, *Science*, 2014, **345**, 1620–1623.

9 O. Einsle, *J. Biol. Inorg. Chem.*, 2014, **19**, 737–745.

10 R. R. Eady, *Chem. Rev.*, 1996, **96**, 3013–3030.

11 A. J. Jasniewski, C. C. Lee, M. W. Ribbe and Y. Hu, *Chem. Rev.*, 2020, **120**, 5107–5157.

12 C. Van Stappen, L. Decamps, G. E. Cutsail, R. Bjornsson, J. T. Henthorn, J. A. Birrell and S. DeBeer, *Chem. Rev.*, 2020, **120**, 5005–5081.

13 R. N. F. Thorneley and D. J. Lowe, Molybdenum Enzymes, ed. T. G. Spiro, Wiley, New York, 1985, pp. 221–284.

14 T. Spatzal, J. Schlesier, E.-M. Burger, D. Sippel, L. Zhang, S. L. A. Andrade, D. C. Rees and O. Einsle, *Nat. Commun.*, 2016, 7, 10902–10902.

15 B. Benediktsson and R. Bjornsson, *Inorg. Chem.*, 2017, **56**, 13417–13429.

16 R. Bjornsson, F. Neese and S. DeBeer, *Inorg. Chem.*, 2017, **56**, 1470–1477.

17 S. J. Yoo, H. C. Angove, V. Papaefthymiou and B. K. Burgess, *J. Am. Chem. Soc.*, 2000, **122**, 4926–4936.

18 C. Van Stappen, R. Davydov, Z.-Y. Yang, R. Fan, Y. Guo, E. Bill, L. C. Seefeldt, B. M. Hoffman and S. DeBeer, *Inorg. Chem.*, 2019, **58**, 12365–12376.

19 C. Van Stappen, A. T. Thorhallsson, L. Decamps, R. Bjornsson and S. DeBeer, *Chem. Sci.*, 2019, **10**, 9807–9821.

20 K. Fisher, W. E. Newton and D. J. Lowe, *Biochemistry*, 2001, **40**, 3333–3339.

21 D. Lukoyanov, B. M. Barney, D. R. Dean, L. C. Seefeldt and B. M. Hoffman, *Proc. Natl. Acad. Sci. U. S. A.*, 2007, **104**, 1451–1455.

22 D. Lukoyanov, Z.-Y. Yang, S. Duval, K. Danyal, D. R. Dean, L. C. Seefeldt and B. M. Hoffman, *Inorg. Chem.*, 2014, **53**, 3688–3693.

23 D. A. Lukoyanov, N. Khadka, Z.-Y. Yang, D. R. Dean, L. C. Seefeldt and B. M. Hoffman, *Inorg. Chem.*, 2018, **57**, 6847–6852.

24 R. Y. Igarashi, M. Laryukhin, P. C. Dos Santos, H.-I. Lee, D. R. Dean, L. C. Seefeldt and B. M. Hoffman, *J. Am. Chem. Soc.*, 2005, **127**, 6231–6241.

25 D. Lukoyanov, N. Khadka, Z.-Y. Yang, D. R. Dean, L. C. Seefeldt and B. M. Hoffman, *J. Am. Chem. Soc.*, 2016, **138**, 10674–10683.

26 V. Hoeke, L. Tociu, D. A. Case, L. C. Seefeldt, S. Raugei and B. M. Hoffman, *J. Am. Chem. Soc.*, 2019, **141**, 11984–11996.

27 D. J. Lowe and R. N. Thorneley, *Biochem. J.*, 1984, **224**, 877–886.

28 R. N. F. Thorneley and D. J. Lowe, *Biochem. J.*, 1984, **224**, 887–894.

29 B. D. Howes, K. Fisher and D. J. Lowe, *Biochem. J.*, 1994, **297**, 261–264.

30 D. Lukoyanov, Z.-Y. Yang, N. Khadka, D. R. Dean, L. C. Seefeldt and B. M. Hoffman, *J. Am. Chem. Soc.*, 2015, **137**, 3610–3615.

31 Z. Y. Yang, N. Khadka, D. Lukoyanov, B. M. Hoffman, D. R. Dean and L. C. Seefeldt, *Proc. Natl. Acad. Sci. U. S. A.*, 2013, **110**, 16327–16332.

32 H. Yang, J. Rittle, A. R. Marts, J. C. Peters and B. M. Hoffman, *Inorg. Chem.*, 2018, **57**, 12323–12330.

33 B. M. Barney, R. Y. Igarashi, P. C. Dos Santos, D. R. Dean and L. C. Seefeldt, *J. Biol. Chem.*, 2004, **279**, 53621–53624.

34 R. Sarma, B. M. Barney, S. Keable, D. R. Dean, L. C. Seefeldt and J. W. Peters, *J. Inorg. Biochem.*, 2010, **104**, 385–389.

35 I. Dance, *ChemBioChem*, 2020, **21**, 1671–1709.

36 T. Lovell, J. Li, T. Liu, D. A. Case and L. Noodleman, *J. Am. Chem. Soc.*, 2001, **123**, 12392–12410.

37 L. Cao, O. Caldararu and U. Ryde, *J. Chem. Theory Comput.*, 2018, **14**, 6653–6678.

38 L. Cao and U. Ryde, *Phys. Chem. Chem. Phys.*, 2019, **21**, 2480–2488.

39 I. Dance, *Chem. Commun.*, 1997, 165–166, DOI: 10.1039/A607136H.

40 T. H. Rod and J. K. Nørskov, *J. Am. Chem. Soc.*, 2000, **122**, 12751–12763.

41 Z. Cao, Z. Zhou, H. Wan, Q. Zhang and W. Thiel, *Inorg. Chem.*, 2003, **42**, 6986–6988.

42 L. C. Seefeldt, I. G. Dance and D. R. Dean, *Biochemistry*, 2004, **43**, 1401–1409.

43 J. Schimpl, H. M. Petrilli and P. E. Blöchl, *J. Am. Chem. Soc.*, 2003, **125**, 15772–15778.

44 P. P. Hallmen and J. Kästner, *Z. Anorg. Allg. Chem.*, 2015, **641**, 118–122.

45 M. L. McKee, *J. Comput. Chem.*, 2007, **28**, 1342–1356.

46 I. Dance, *Dalton Trans.*, 2019, **48**, 1251–1262.

47 I. Dance, *Dalton Trans.*, 2022, **51**, 15538–15554.

48 D. Sippel, M. Rohde, J. Netzer, C. Trncik, J. Gies, K. Grunau, I. Djurdjevic, L. Decamps, S. L. A. Andrade and O. Einsle, *Science*, 2018, **359**, 1484–1489.

49 W. Kang, C. C. Lee, A. J. Jasniewski, M. W. Ribbe and Y. Hu, *Science*, 2020, **368**, 1381–1385.

50 K. L. Skubi and P. L. Holland, *Biochemistry*, 2018, **57**, 3540–3541.

51 T. M. Buscagan and D. C. Rees, *Joule*, 2019, **3**, 2662–2678.

52 A. T. Thorhallsson, B. Benediktsson and R. Bjornsson, *Chem. Sci.*, 2019, **10**, 11110–11124.

53 Y. Pang and R. Bjornsson, *Inorg. Chem.*, 2023, **62**, 5357–5375.

54 S. Raugei, L. C. Seefeldt and B. M. Hoffman, *Proc. Natl. Acad. Sci. U. S. A.*, 2018, **115**, 10521–10530.

55 D. A. Lukoyanov, Z.-Y. Yang, D. R. Dean, L. C. Seefeldt, S. Raugei and B. M. Hoffman, *J. Am. Chem. Soc.*, 2020, **142**, 21679–21690.

56 I. Dance, *J. Am. Chem. Soc.*, 2007, **129**, 1076–1088.

57 I. Dance, *Z. Anorg. Allg. Chem.*, 2015, **641**, 91–99.

58 I. Dance, *Dalton Trans.*, 2021, **50**, 18212–18237.

59 I. Dance, *Dalton Trans.*, 2022, **51**, 12717–12728.

60 P. E. M. Siegbahn, *Phys. Chem. Chem. Phys.*, 2019, **21**, 15747–15759.

61 W.-J. Wei and P. E. M. Siegbahn, *Chem. – Eur. J.*, 2022, **28**, e202103745–e202103745.

62 A. T. Thorhallsson and R. Bjornsson, *Chem. – Eur. J.*, 2021, **27**, 16788–16800.

63 H. Jiang, O. K. G. Svensson and U. Ryde, *Inorg. Chem.*, 2022, **61**, 18067–18076.

64 M. Rohde, D. Sippel, C. Trncik, S. L. A. Andrade and O. Einsle, *Biochemistry*, 2018, **57**, 5497–5504.

65 P. E. M. Siegbahn, *J. Comput. Chem.*, 2018, **39**, 743–747.

66 L. Cao and U. Ryde, *J. Chem. Theory Comput.*, 2020, **16**, 1936–1952.

67 D. Lukoyanov, N. Khadka, D. R. Dean, S. Raugei, L. C. Seefeldt and B. M. Hoffman, *Inorg. Chem.*, 2017, **56**, 2233–2240.

68 L. Cao, O. Caldararu and U. Ryde, *J. Phys. Chem. B*, 2017, **121**, 8242–8262.

69 L. Cao and U. Ryde, *Int. J. Quantum Chem.*, 2018, **118**, e25627 (25616 pages).

70 B. M. Barney, J. McClead, D. Lukoyanov, M. Laryukhin, T.-C. Yang, D. R. Dean, B. M. Hoffman and L. C. Seefeldt, *Biochemistry*, 2007, **46**, 6784–6794.

71 J. A. Maier, C. Martinez, K. Kasavajhala, L. Wickstrom, K. E. Hauser and C. Simmerling, *J. Chem. Theory Comput.*, 2015, **11**, 3696–3713.

72 W. L. Jorgensen, J. Chandrasekhar, J. D. Madura, R. W. Impey and M. L. Klein, *J. Chem. Phys.*, 1983, **79**, 926–935.

73 L. Cao and U. Ryde, *J. Biol. Inorg. Chem.*, 2020, **25**, 521–540.

74 L. Hu and U. Ryde, *J. Chem. Theory Comput.*, 2011, **7**, 2452–2463.

75 C. I. Bayly, P. Cieplak, W. D. Cornell and P. A. Kollman, *J. Phys. Chem.*, 1993, **97**, 10269–10280.

76 F. Furche, R. Ahlrichs, C. Hättig, W. Klopper, M. Sierka and F. Weigend, *Wiley Interdiscip. Rev.: Comput. Mol. Sci.*, 2014, **4**, 91–100.

77 J. Tao, J. P. Perdew, V. N. Staroverov and G. E. Scuseria, *Phys. Rev. Lett.*, 2003, **91**, 146401–146401.

78 J. W. Furness, A. D. Kaplan, J. Ning, J. P. Perdew and J. Sun, *J. Phys. Chem. Lett.*, 2020, **11**, 8208–8215.

79 V. N. Staroverov, G. E. Scuseria, J. Tao and J. P. Perdew, *J. Chem. Phys.*, 2003, **119**, 12129–12137.

80 A. D. Becke, *Phys. Rev. A*, 1988, **38**, 3098–3100.

81 C. Lee, W. Yang and R. G. Parr, *Phys. Rev. B: Condens. Matter Mater. Phys.*, 1988, **37**, 785–789.

82 A. D. Becke, *J. Chem. Phys.*, 1993, **98**, 1372–1372.

83 B. Benediktsson and R. Bjornsson, *J. Chem. Theory Comput.*, 2022, **18**, 1437–1457.

84 A. Schäfer, H. Horn and R. Ahlrichs, *J. Chem. Phys.*, 1992, **97**, 2571–2577.

85 K. Eichkorn, O. Treutler, H. Öhm, M. Häser and R. Ahlrichs, *Chem. Phys. Lett.*, 1995, **240**, 283–289.

86 K. Eichkorn, F. Weigend, O. Treutler and R. Ahlrichs, *Theor. Chem. Acc.*, 1997, **97**, 119–124.

87 E. Caldeweyher, S. Ehlert, A. Hansen, H. Neugebauer, S. Spicher, C. Bannwarth and S. Grimme, *J. Chem. Phys.*, 2019, **150**, 154122–154122.

88 L. Cao and U. Ryde, *J. Catal.*, 2020, **391**, 247–259.

89 R. Bjornsson, F. A. Lima, T. Spatzal, T. Weyhermüller, P. Glatzel, E. Bill, O. Einsle, F. Neese and S. DeBeer, *Chem. Sci.*, 2014, **5**, 3096–3103.

90 D. J. Lowe, R. R. Eady and R. N. F. Thorneley, *Biochem. J.*, 1978, **173**, 277–290.

91 C. Greco, P. Fantucci, U. Ryde and L. D. Gioia, *Int. J. Quantum Chem.*, 2011, **111**, 3949–3960.

92 R. K. Szilagyi and M. A. Winslow, *J. Comput. Chem.*, 2006, **27**, 1385–1397.

93 A. Klamt and G. Schüürmann, *J. Chem. Soc., Perkin Trans. 2*, 1993, 799–805.

94 A. Schäfer, A. Klamt, D. Sattel, J. C. W. Lohrenz and F. Eckert, *Phys. Chem. Chem. Phys.*, 2000, **2**, 2187–2193.

95 A. Klamt, V. Jonas, T. Bürger and J. C. W. Lohrenz, *J. Phys. Chem. A*, 1998, **102**, 5074–5085.

96 U. Ryde, *J. Comput.-Aided Mol. Des.*, 1996, **10**, 153–164.

97 U. Ryde and M. H. M. Olsson, *Int. J. Quantum Chem.*, 2001, **81**, 335–347.

98 N. Reuter, A. Dejaegere, B. Maigret and M. Karplus, *J. Phys. Chem. A*, 2000, **104**, 1720–1735.

99 L. Hu, P. Söderhjelm and U. Ryde, *J. Chem. Theory Comput.*, 2011, **7**, 761–777.

100 L. Cao and U. Ryde, *Front. Chem.*, 2018, **6**, 89–89.

101 L. Goerigk, A. Hansen, C. Bauer, S. Ehrlich, A. Najibi and S. Grimme, *Phys. Chem. Chem. Phys.*, 2017, **19**, 32184–32215.

102 I. Dance, *Mol. Simul.*, 2018, **44**, 568–581.

103 M. Torbjörnsson and U. Ryde, *Electron. Struct.*, 2021, **3**, 34005–34005.

104 M. G. Delcey, K. Pierloot, Q. M. Phung, S. Vancoillie, R. Lindh and U. Ryde, *Phys. Chem. Chem. Phys.*, 2014, **16**, 7927–7938.

105 G. Dong, Q. M. Phung, S. D. Hallaert, K. Pierloot and U. Ryde, *Phys. Chem. Chem. Phys.*, 2017, **19**, 10590–10601.

106 I. Dance, *Dalton Trans.*, 2015, **44**, 9027–9037.

107 H. Jiang, O. K. G. Svensson and U. Ryde, *Molecules*, 2023, **28**, 65.